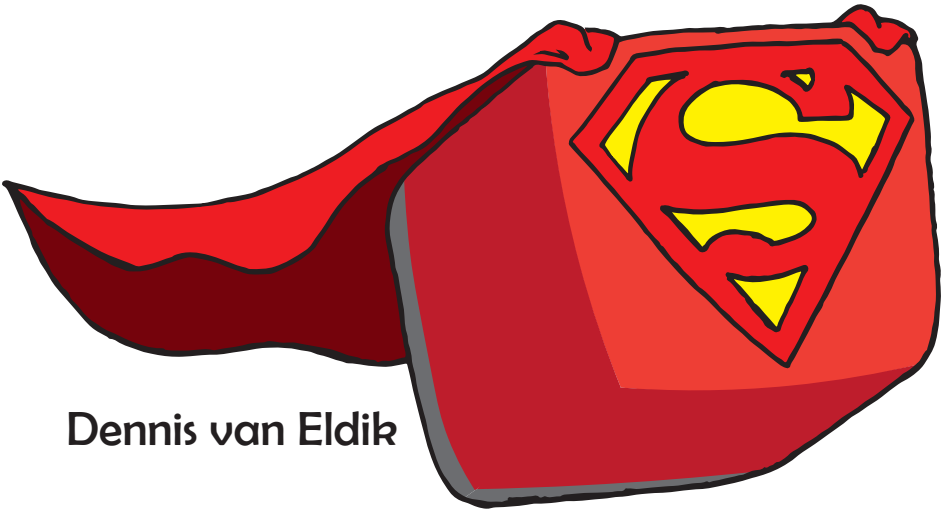

Dennis van Eldik

self-propelling superballs

Master thesis

Self-propelling Superballs

Dennis van Eldik

Under the supervision of:
Samia Ouhajji
Dr. Andrei V. Petukhov
Prof. Dr. Albert P. Philipse

Van 't Hoff Laboratory for Physical & Colloid Chemistry
Utrecht University
Netherlands
December 22, 2016

ABSTRACT

This work demonstrates the synthesis and characterisation of novel self-propelling colloidal superballs. The particles consist of haematite cubes with a silica shell, coated on one face with a thin layer of platinum. Platinum catalyses the decomposition of hydrogen peroxide, causing a concentration gradient around the particle that propels the particle forward.

The goal of this research was to synthesise these self-propelling superballs and to quantify their single-particle behaviour. Various values and parameters were investigated to determine the effect of cubicity on the motion of active particles, including the diffusion coefficient, persistence time and velocity. In addition, active motion as a function of peroxide concentration and temperature was mapped.

Self-propelling superballs of roughly 1 µm in size were successfully synthesised, with their effective diffusion coefficient increasing with peroxide concentration and temperature. However, the developed analysis method, involving fitting of the mean squared displacement with a diffusion equation, was not robust enough to quantitatively describe swimming motion.

CONTENTS

1. GENERAL INTRODUCTION

The research field of self-propelled particles is rapidly expanding [1]. Particles are called self-propelling if they are able to move autonomously in fluids of low Reynolds number. At low Reynolds number, viscous forces dominate over inertia forces, which makes swimming processes fundamentally different. To illustrate this: while an oil tanker needs at least 15 minutes to come to a full stop in full reverse drive, a bacterium stops coasting after about 0.3 µs after switching off its propulsion mechanism [2].

There are numerous examples of self-propelled particles in nature, for example bacteria [3] and spermatozoa [4], but also birds [5] and fish [6] or even people [7] can be considered self-propelling particles.

Numerous examples of artificial self-propelling particles, often called 'microswimmers' or colloidal swimmers, can be found in literature. Artificial colloidal swimmers may find applications in, for example, targeted cargo transport or drug delivery [8, 9]. These self-propelling particles are driven by, for example, diffusiophoresis [10, 11], electrophoresis [12], magnetically induced thermophoresis [13], or using bacteria [14, 15].

The most commonly used method to make particles active is by coating them with platinum. Platinum catalyses the decomposition of hydrogen peroxide, causing particles to swim by creating a concentration gradient around the particle, effectively using H_2O_2 as a fuel.

Ke and co-workers [10] investigated the self-propelled motion of Pt-coated silica spheres (1 µm diameter) in hydrogen peroxide solutions. Optical microscopy was used to observe the motion of the particles, as well as to determine the relative position of the platinum side in order to relate the direction of motion to the direction of the platinum. Figure 1.1 illustrates the directional analysis that was performed.

The authors concluded that the particles moved away from the platinum side and that the particle motion can be described as two regimes: a ballistic regime, where the particle moves straight ahead at short times; and an 'enhanced Brownian' regime at times longer than the rotational

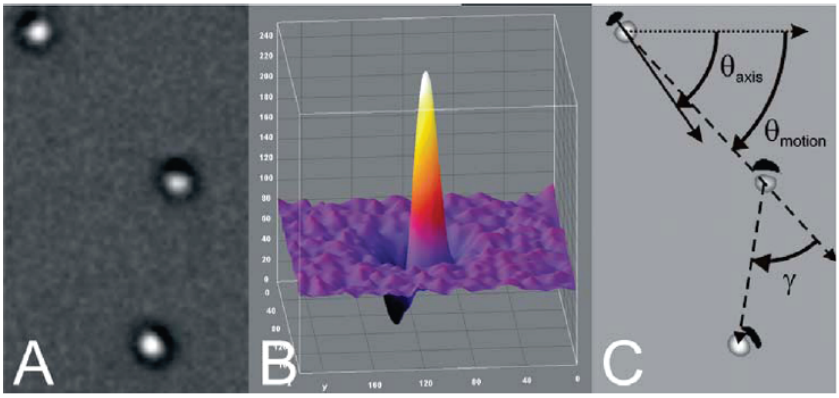

Fig. 1.1: (A) Overlay of three sequential optical micrographs of a half-coated Pt-silica particle undergoing autonomous motion. Sequences of micrographs were flat-field corrected to remove background intensities. (B) Surface plot of transmitted light intensity for a single Janus particle. (C) Segmented and background subtracted images of particles from (A) highlighting the silica region (bright) and the Pt-coated region (dark), along with the angles and trajectories that are used in the motion analysis. Reproduced from [10].

diffusion time.

Palacci et al [16] studied so-called 'living crystals', formed by light-activated colloidal swimmers, see Figure 1.2. The active particles in their work consisted of a haematite cube, partly encapsulated by a TPM sphere, so that one face of haematite is exposed to the solvent. These particles undergo Brownian diffusion in white bright-field illumination, but undergo self-propulsion in hydrogen peroxide under illumination with blue light of 430 nm. Palacci et al studied the formation, breaking and motion in external fields of the dynamic two-dimensional crystals formed by the active particles.

Previous research has mainly focused on spherical [17, 10] and rod-like [18, 19] particles. To the best of our knowledge, no experimental work has been performed on cube-like active particles, in particular superball-shaped particles. Superballs are shapes somewhere between a sphere and a cube, essentially a cube with rounded corners and edges. This work will focus on superball-shaped silica-coated haematite particles of roughly

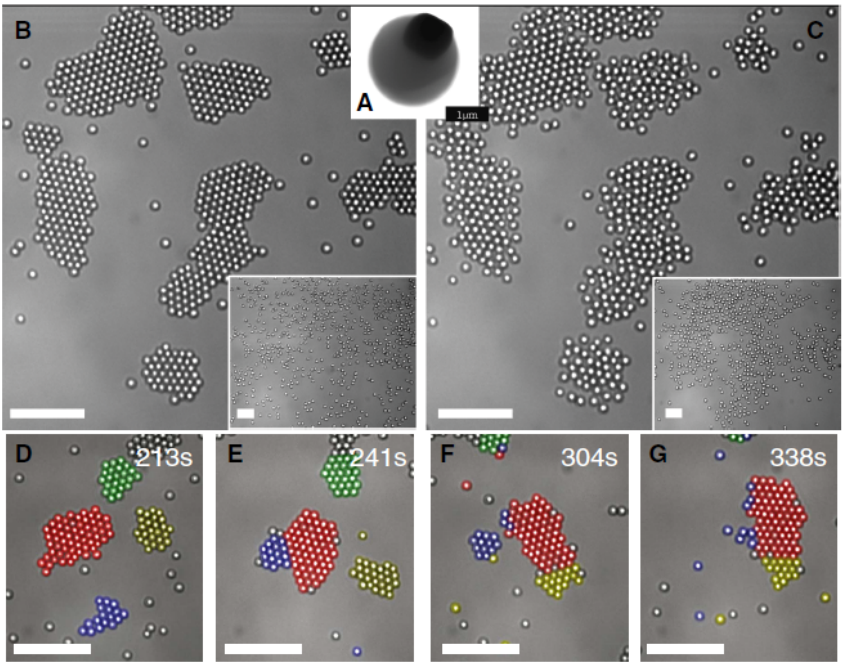

Fig. 1.2: (A) Scanning electron microscopy (SEM) of the bimaterial colloid: a TPM polymer colloidal sphere with protruding hematite cube (dark). (B) Living crystals assembled from a homogeneous distribution (inset) under illumination by blue light. (C) Living crystals melt by thermal diffusion when light is extinguished: Image shows system 10 s after blue light is turned off (inset, after 100 s). (D to G) The false colors show the time evolution of particles belonging to different clusters. The clusters are not static but rearrange, exchange particles, merge (D→F), break apart (E→F), or become unstable and explode (blue cluster, F→G). For (B) to (G), the scale bars indicate 10 µm. The solid area fraction is $\Phi_s \approx 0.14$. Reproduced from [16].

1 µm in size, which are made self-propelling by coating one face with platinum, analogous to the work of Ke et al, among others.

One advantage of using haematite cubes as a basis for the particles is the fact that the colloids are large and have large enough contrast to be observed with optical microscopy, making analysis more convenient. Another reason why haematite is interesting to use, while not further explored in this thesis, is that haematite is a weakly magnetic material. The colloids may be manipulated by external magnetic fields to form interesting structures. Thirdly, the superball shape can influence self-assembly and induces directionality in various ways [20].

The original idea for this project was to create linear chains of these particles using magnetic fields to mimic bacterial swimming motion. However, achieving linear chains of active colloids proved more difficult than initially assumed. Instead, we focused on single-particle motion only. In this work, we make the first steps to establish a quantitative measure for swimming motion, in order to compare self-propelling motion of superball particles to particles of other shapes and sizes.

In this thesis, I will first cover some theoretical background, followed by a description of the synthesis of the swimming superballs. Optical microscopy and particle tracking are used to study the motion of the particles in water and various concentrations of H_2O_2 at different temperatures. Values for the *diffusion coefficient*, *velocity* and *persistence time* are calculated in different ways, in order to develop a comparison method for active particles of different shapes and sizes. Finally, conclusions are drawn and an outlook is given for further research.

2. THEORETICAL BACKGROUND

2.1 Haematite superballs

The family of superballs smoothly interpolates shapes between cubes and spheres. Their rounded contour can be represented by [21]:

$$\left|\frac{x}{a}\right|^m + \left|\frac{y}{b}\right|^m + \left|\frac{z}{c}\right|^m \leq 1 \tag{2.1}$$

where m is the shape parameter and a is half the edge length. A higher m-value denotes a more cubic shape, with $m \to \infty$ for a perfect cube, and $m = 2$ for a perfect sphere. Cubic colloids with rounded edges and corners can generally be approximated as superballs [22]. Figure 2.1 shows superballs with a range of shape factors.

The particles used in this work are haematite cubes, first synthesised by Sugimoto et al. [23], with a silica layer grown around [24]. These particles have a typical edge length of about 1 µm, and a shape factor of $m = 2.5$–4.

Haematite is the mineral form of iron(III) oxide (Fe_2O_3). The name haematite is derived from the Greek word for blood, *αἱμα*, since the powdered mineral can be used as a blood red pigment. Haematite is a canted anti-ferromagnetic material above the Morin transition (250 K) and below the Néel temperature (948 K). Spin canting is a phenomenon where spins are tilted by a small angle about their axis, instead of being exactly anti-parallel. This effect causes a (small) net magnetisation at room temperature. The magnetic dipole of a haematite cube is directed along the body diagonal, tilted by about 14° [25].

To determine the m-value of a superball, one can perform a contour fit of the 2D projection of the superball (the 2D equivalent is called a superdisk) obtained by TEM imaging [21]. For this method, individual particles that are lying flat on a sample grid are essential.

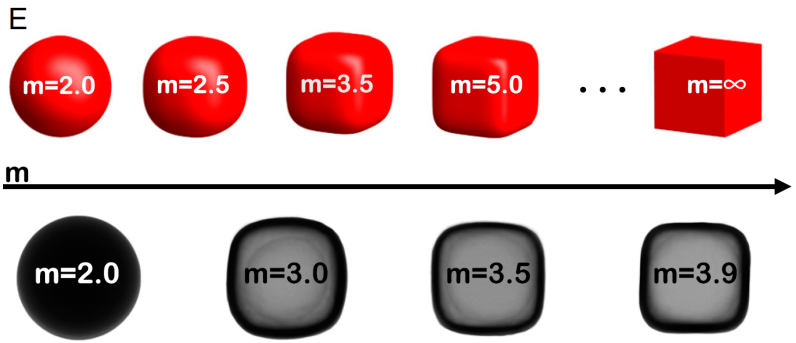

Fig. 2.1: Top: superball shapes with varying shape factor m. $m = 2$ for a perfect sphere, $m \to \infty$ for a cube. Bottom: TEM-images of (hollow) silica particles with various shape factors [22].

A simpler approach involves the ratio of the edge length to the face diagonal L, as follows [26]:

$$L = \sqrt{8}a \left(\frac{1}{2}\right)^{1/m} \tag{2.2}$$

However, the contour fit can better compensate for particles that are not lying perfectly flat (by considering the case where a and b, the semi-axes of the superball are not equal), so that method is most often used to determine the shape factor.

2.2 Active Brownian Motion

The motion of self-propelling particles can be explained as consisting of two parts: the phoretic motion induced by the self-propulsion and the intrinsic, random motion every particle exhibits below micrometer scale. This section will first describe this random motion, then move on to propelled motion. Finally the two regimes are combined to obtain one equation for describing the motion of self-propelling colloids, following the example of Howse et al. [17].

2.2.1 Brownian motion

On a micro scale, objects suspended in a fluid have an intrinsic translational and rotational motion due to thermal fluctuations, known widely as Brownian motion. Brownian motion is typically characterised by the (translational) diffusion coefficient D_0, following from the famous Stokes-Einstein relation:

$$D_0 = \frac{k_\mathrm{B}T}{6\pi\eta R} \tag{2.3}$$

for spherical particles with radius R dispersed in a fluid with viscosity η. $k_\mathrm{B} = 1.38\,\mathrm{J\,K^{-1}}$ is the Boltzmann constant and T is the absolute temperature in K. Similar to the translational diffusion coefficient, the rotational diffusion coefficient D_R (and the rotation time τ_R) can be determined from:

$$D_\mathrm{R} = \tau_R^{-1} = \frac{k_\mathrm{B}T}{8\pi\eta R^3} \tag{2.4}$$

Note that equations 2.3 and 2.4 only hold true for perfect spheres, so the actual value for the diffusion coefficient will change slightly depending on the actual shape of the particle. For superballs with a shape factor of $m \approx 3$, the translational diffusion coefficient does not differ significantly from that of a sphere of equal size [27]. For rotational diffusion, since the coefficient scales with R^3 instead of linearly, the difference is expected to be larger. However, an exact determination of the rotational diffusion coefficient for superball particles remains an unsolved challenge. Preliminary calculations by Tuinier show that the (rotational and translational) diffusion coefficient of superballs deviate from that of spheres by less than 10 % [28].

2.2.2 Mean squared displacement

To describe the motion of colloids, we can use the mean squared displacement. The mean squared displacement (MSD) is a measure for the mean distance a particle has 'explored' with respect to a reference position at a certain time. It is defined as

$$\mathrm{MSD} \equiv \left\langle (r - r_0)^2 \right\rangle = \frac{1}{N}\sum_{n=1}^{N} \left(r_n(t) - r_n(0)\right)^2 \tag{2.5}$$

where N is the number of particles being averaged, $r_n(0) = r_0$ is the reference position of each particle and $r_n(t)$ the position of the particle at time t.

Einstein related the diffusion coefficient of Brownian particles to the mean squared displacement [29], and for truly stochastic motion the mean squared displacement can be calculated as

$$\mathrm{MSD} \equiv \left\langle \boldsymbol{r}^2 \right\rangle = 2dD_0t \tag{2.6}$$

with d the dimensionality of the system.

The MSD is experimentally determined in this work via particle tracking. Equation 2.5 is used to calculate the MSD of each particle, then equation 2.6 is fitted to the MSD to obtain the value for D_0. $d = 2$ is used, since we observe two-dimensional motion (see section 3.5 for more details).

The MSD of a non-active (Brownian) particle scales approximately with t, indicating *diffusive* motion. For active particles, the short-term MSD scales with t^2 as the particle moves *ballistically*, i.e. in a straight line. At observation times longer than the rotational diffusion, the particles will behave effectively diffusive, with the MSD scaling linearly with time again.

2.2.3 Diffusiophoresis

Using the MSD, we can describe the active motion of self-propelling particles. The particles in this work swim via diffusiophoresis. Diffusiophoresis is the spontaneous motion of dispersed particles induced by a concentration gradient of dissolved substances, see Figure 2.2. It was first theoretically predicted and experimentally established by Derjaguin [30]. The chemical energy of the gradient is converted into mechanical energy of colloids moving through a fluid [31].

A simple way to predict self-diffusiophoresis does not exist [31], as the concentration gradient around the particle varies greatly, the composition and thickness of the platinum layer is not homogeneous, and the chemical environment surrounding the particle changes every second.

The active motion as a result of diffusiophoresis can be described by means of the MSD. The equation describing the full range of motion of a self-propelling particle is shown by Howse to be [17]:

$$\left\langle \mathbf{r}^2 \right\rangle = 4\left(D_0 + \frac{1}{4}v^2\tau\right)t + v^2\tau\left[e^{-\frac{2t}{\tau}} - 1\right] \tag{2.7}$$

with v the swimming velocity and τ the persistence time, which are related via the persistence length $l = v\tau$. The persistence time is believed to be

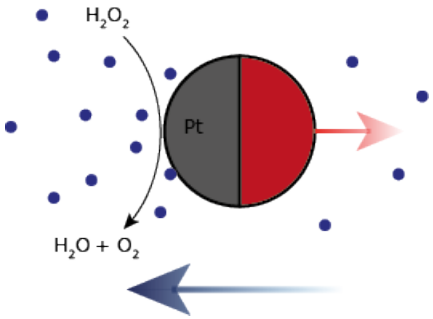

Fig. 2.2: Self-diffusiophoresis. The platinum film (dark gray) produces a gradient of oxygen (blue), propelling the particle away from the high concentration.

related to the rotational diffusion of the particle; the typical time it takes for a self-propelling particle to rotate is the typical time at which it will lose its directionality.

The short-time limit ($t \ll \tau$) of this equation can be approximated as:

$$\left\langle \mathbf{r}^2 \right\rangle \approx 4D_0 t + v^2 t^2 \tag{2.8}$$

Here the particle motion is ballistic, so $\left\langle \mathbf{r}^2 \right\rangle \sim t^2$.

At long time scales ($t \gg \tau$), the motion can be viewed as diffusive ($\left\langle \mathbf{r}^2 \right\rangle \sim t$), with a higher effective or apparent diffusion coefficient D_{eff}, and can be described by:

$$\left\langle \mathbf{r}^2 \right\rangle \approx 4D_{\text{eff}} t. \tag{2.9}$$

2.2.4 Catalysed decomposition of hydrogen peroxide

The concentration gradient in our system, needed for diffusiophoresis, is created by the heterogeneously catalysed decomposition of hydrogen peroxide at the platinum surface. Hydrogen peroxide is decomposed to water and oxygen:

$$2\ \mathrm{H_2O_2} \xrightarrow{\mathrm{Pt}} 2\ \mathrm{H_2O} + \mathrm{O_2} \tag{2.10}$$

No consensus has been reached about the exact mechanism of the catalysis, although various mechanisms have been proposed [32, 11, 33]. The prevailing explanation [11, 17] is the formation of a $\mathrm{Pt(H_2O_2)}$ complex at

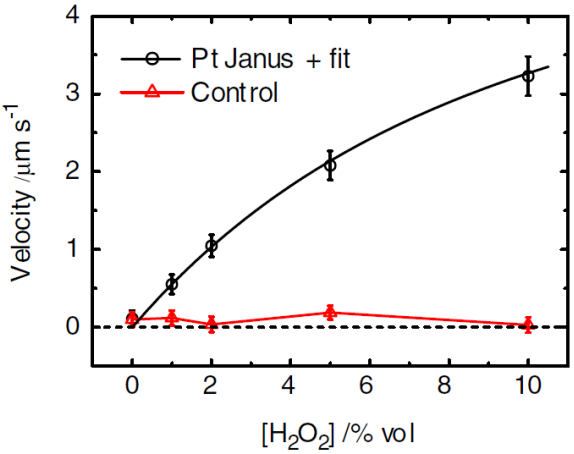

Fig. 2.3: Janus particle swimming velocity versus H_2O_2 concentration, suggesting Michaelis-Menten type kinetics (solid black line) for the H_2O_2 decomposition. Reproduced from [17].

the platinum surface at a rate per unit area $k_1[H_2O_2]$, followed by the decomposition of the peroxide into water and oxygen at a rate per unit area k_2. This mechanism would lead to Michaelis-Menten-type behaviour for the reaction rate (and the resulting particle velocity), which corresponds well with experimental data [17], see Figure 2.3. Increasing the peroxide concentration or the temperature both lead to a higher decomposition rate.

2.3 Peltier element

In this work, a Peltier element is used to control the temperature of the sample holder during microscopy experiments, see section 3.5. A Peltier element (or Peltier-Seebeck element) is an electronic component which can be used to transport heat from a cold to a warm place, or to generate electricity from a heat gradient.

The Peltier effect is named after Jean Charles Athanase Peltier, who discovered in 1834 that when an electrical current flows through the junction of two conductors (N-type and P-type semiconductors), heat may be generated or removed at the junction [34]. Applying multiple Peltier units

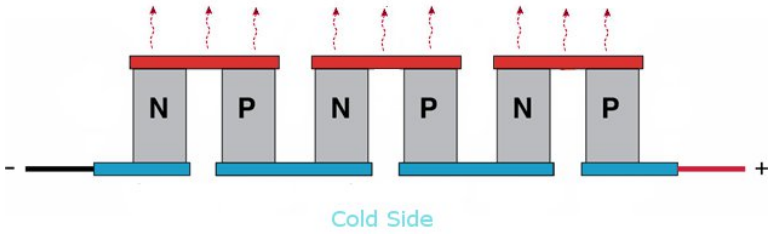

Fig. 2.4: Diagram of a Peltier element. Heat is generated at one side (red), while heat is absorbed on the other side (blue).

in series creates a heat pump, which can be used to either heat or cool. A diagram of a peltier element is shown in Figure 2.4.

3. EXPERIMENTAL DETAILS

3.1 Materials

Table 3.1 lists all commercial materials used in the project, along with some properties and their supplier.

Tab. 3.1: Commercially obtained materials used in this project.

Name, purity (acronym)	**Supplier**
N,N-Dimethylformamide, $\geq$ 99.8% (DMF)	Sigma Aldrich
Ethanol, 100% (EtOH)	Interchema
Hydrochloric acid, 37% (HCl)	PA Merck
Hydrogen peroxide, 35% (H_2O_2)	Fisher Scientific
Hydrogen peroxide, $\geq$ 35% (H_2O_2)	Sigma Aldrich
Iron(III) chloride hexahydrate, ($FeCl_3 \cdot H_2O$)	Sigma Aldrich
Platinum trace metal basis, 99.9% (Pt)	Sigma Aldrich
Polyvinylpyrrolidone, 10 kg mol^{-1}(PVP)	Sigma Aldrich
Polyvinylpyrrolidone, 40 kg mol^{-1} (PVP)	Sigma Aldrich
Potassium hydroxide, powder (KOH)	VWR International
Sodium hydroxide, pellets (NaOH)	VWR International
Tetraethyl orthosilicate, $\geq$ 99.0% (TEOS)	Sigma Aldrich
Tetramethylammonium hydroxide, 20% (TMAH)	Sigma Aldrich

In the text where water is mentioned, the water used is purified by a Milli-Q filter. All chemicals are stored at ambient conditions, except for hydrogen peroxide which was stored in the fridge.

3.2 Preparation of active superballs

This section will describe the synthesis of the active colloidal particles. First, haematite cubes were synthesised and subsequently coated with a

layer of silica. The silica minimized dipole-dipole attractions between the particles, so we can observe single-particle motion with as few as possible interactions. After the silica coating, the particles were deposited on a glass slide as a monolayer for platinum coating. The monolayer was needed to coat all particles evenly on one face. Finally, the particles were redispersed in water/H_2O_2 for experiments.

The protocol for the synthesis of silica-coated haematite cubes is based on the latest works of our group [21, 35, 36].

3.2.1 Haematite cube synthesis

For the synthesis of haematite cubes of roughly 800 nm in size, first 20.08 g of sodium hydroxide pellets were dissolved in roughly 60 mL water in a volumetric flask. Due to the mixing of a strong base with water, the mixture heated up. After approximately 12 hours, the mixture was cooled to room temperature and the flask was filled up to 100 mL.

As the ratio of iron to base ions greatly influences the size and shape of the cubes, it is important to know exactly how much iron is used for the synthesis. Therefore, 50.29 g of iron(iii) oxide hexahydrate was weighed as quickly as possible while keeping the iron oxide container under a nitrogen flow to prevent the highly hygroscopic salt to absorb water. 100 mL water was added to the salt and the mixture was sonicated for 20 minutes. The NaOH solution was added to this mixture in about 26 seconds while stirring magnetically at the highest speed. The mixture was stirred for another 10 minutes, and then the mixture was placed in a pre-heated oven at 100 °C for 8 days.

After the aging period, the haematite cubes were washed multiple times with water, until the pH of the supernatant reached a steady pH of 5. Centrifugation was done at 800 g for 30 minutes. The cubes were stored in water in a 250 mL Pyrex bottle.

3.2.2 Silica-coating of haematite cubes

Prior to the silica coating, the haematite cubes are covered with PVP. This prevents aggregation of the particles and improves the silica growth. First, a solution of 5.32 g PVP (40 kg mol^{-1}) in 150 mL water was prepared and sonicated to ensure complete dissolution. This solution was added to 20 mL of the haematite cube dispersion (5.4 wt%) and was stirred magnetically overnight. The mixture was then centrifuged for 30 minutes at

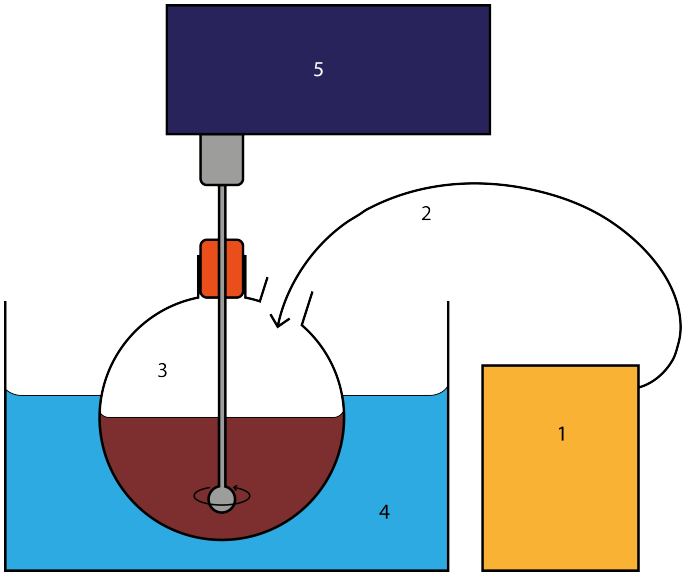

Fig. 3.1: Schematic set-up used for the silica coating. The 1:1 TEOS : ethanol mixture is led from the peristaltic pump **(1)**, through a tube **(2)**, to the round-bottom flask **(3)** inside an ultrasonic bath **(4)**. The mixture is stirred with an overhead stirrer **(5)**.

800 g. The residue was washed thrice to remove excess PVP by redispersing in 100 mL (first step) or 20 mL (second and third step) ethanol.

For the growth of silica on the superballs, a set-up as schematically depicted in Figure 3.1 was used. A 1-liter two-neck round-bottom flask **(3)** is suspended in an ultrasonic bath **(4)**, with an overhead stirrer **(5)** attached. While sonicating and mechanically stirring, 380 mL ethanol was added to the flask, along with 66 mL miliQ water, 10 mL of an aqueous solution of TMAH (1% w/w) and 20 mL of the PVP-coated haematite cubes.

A mixture of 15 mL TEOS and 10 mL ethanol was added dropwise using a peristaltic pump **(1)** in 45 minutes (pump speed set to 5 rpm). The mixture was sonicated and mechanically stirred for another 2 hours, and stirred without sonication overnight. The product was centrifuged (30 min, 800 g) and washed three times with ethanol. The silica coated cubes were stored in ethanol.

3.2.3 Hollow silica cubes

The synthesised silica-haematite superballs can be made hollow, allowing for various applications such as cargo transport. To remove the haematite core, the silica coated cubes are stirred in a solution of hydrochloric acid (6 M) for about 24 hours. The exact time it takes for the cores to dissolve, depends on the size of the cubes. The acid might need to be replaced, if the solution is still coloured orange after 24 hours.

When the solution is turned yellow, the cores are completely dissolved. The resulting particles appear white. The hollow cubes were centrifuged and washed with ethanol several times until a steady pH was obtained (around 5–6). The hollow silica superballs were stored in ethanol.

3.2.4 Monolayer deposition

For the deposition of a dilute monolayer of particles, first a glass coverslip (20 mm × 20 mm #1.5) was cleaned by rinsing with water and ethanol. The coverslip was placed on a flat surface, tilted very slightly against the horizontal (around 3°), and small droplets of 10 µL aqueous particle dispersion (0.5 wt%) were pipetted on the glass. The small tilt tends to yield higher quality monolayers [37]. The idea behind the tilt is that it causes a deformation of the droplet so that nucleation of the monolayer starts at the upper edge of the droplet and the crystallisation proceeds downward in a directional fashion.

A schematic representation of the set-up is shown in Figure 3.2. The coverslip was covered with a crystallisation dish to prevent air flow and to slow down evaporation and the droplets were left to dry overnight. The quality of the monolayer was evaluated by looking with optical microscopy or scanning electron microscopy (SEM). A suitable monolayer for sputter coating should have no overlapping particles, so that all particles will be equally coated with platinum on one face.

3.2.5 Platinum coating

The coverslip was taped with adhesive tape to the rotary stage of a Cressington 108 sputter coater, with rotation switched on at standard speed. The sputter chamber was flushed with argon and evacuated to 0.08 mbar. A layer of 5 nm platinum was sputtered on the slide (measured with a Cressington MTM-10 thickness monitor).

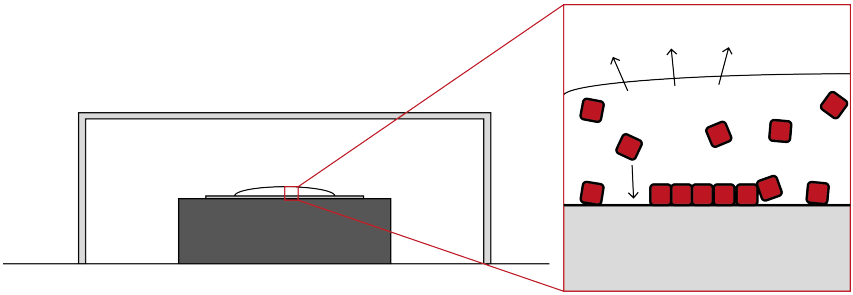

Fig. 3.2: Schematic representation of the monolayer deposition set-up. Water evaporates, causing the particles to settle on the glass in an organised fashion.

To redisperse the platinum-coated particles, the coated coverslips were simply laid inside a Falcon tube or beaker with water so that the coverslips were just submerged, and sonicated for about one hour. The actual time needed to completely remove all particles from the slide varied between samples, but never exceeded 4 hours. Silica will be slowly etched if stored in water, so if long-term storage was desired, ethanol was used instead of water. For short-term storage, water was more practical, since all experiments were performed in aqueous conditions.

3.3 Characterisation

Transmission electron microscopy (TEM) was used to determine the size and shape factor of the particles. For TEM-experiments, a Philips TECHNAI 10 was used. Before an experiment, a sample grid was prepared by placing a droplet of diluted particle dispersion on a TEM-grid and letting it dry under a lamp.

Scanning electron microscopy (SEM) was performed using a Phenom Pro scanning electron microscope.

3.4 'Swimming' superballs

A stock solution of the desired hydrogen peroxide concentration was prepared, and TMAH was added as a base until pH = 8 was reached for optimal particle stability. The total amount of added base may vary be-

tween experiments, but the pH was always tested to be 8. For a typical microscopy experiment, 5 µL particles dispersion (around 0.005 wt%) was added to 195 µL H_2O_2 stock solution in an eppendorf tube and sonicated for 5 minutes before it was added to the microscopy sample cell. The concentration of particles was deliberately very low for the experiments in order to exclude particle interactions, because we want to observe single-particle motion.

3.5 Microscopy and tracking

A motorized Nikon Ti-Eclipse inverted optical microscope was used for experiments, equipped with a Hamamatsu camera and controlled by the NIS-Elements software.

3.5.1 Sample cell

The microscopy sample cell is shown schematically in Figure 3.3. It consists of a glass coverslip (24 mm × 60 mm, #1.5) with a bottomless vial (0.5 mL) glued on top. The coverslip is glued to the bottom of a thick microscopy glass slide, with a hole drilled in the center that fits around the vial. The vial, in turn, fits inside an aluminium block, where a Peltier element can be attached for temperature control. A hole in the side of the block allows for a temperature sensor to probe the temperature of the vial. This sensor is connected to a Peltier controller, where a desired temperature can be set. Control experiments showed that the temperature of the outside of the vial (measured by the sensor) was equal to the temperature of the fluid after a few seconds of equilibration.

The heating used an input voltage of 24 V and a 0.10 A current. After an equilibration time of roughly one minute, the temperature oscillated around the set-point with $\Delta T = \pm\, 0.1\,^{\circ}\mathrm{C}$.

3.5.2 Video recording

To obtain video recordings of the particle motion, a 60x magnification was used (40x objective with 1.5x intermediate objective), and a camera frame rate of 30–60 frames per second. The typical length of a video was 1500 frames, or 50 s. It was found that a frame rate of 30 fps is sufficient to accurately track the particles. The haematite superballs have a higher

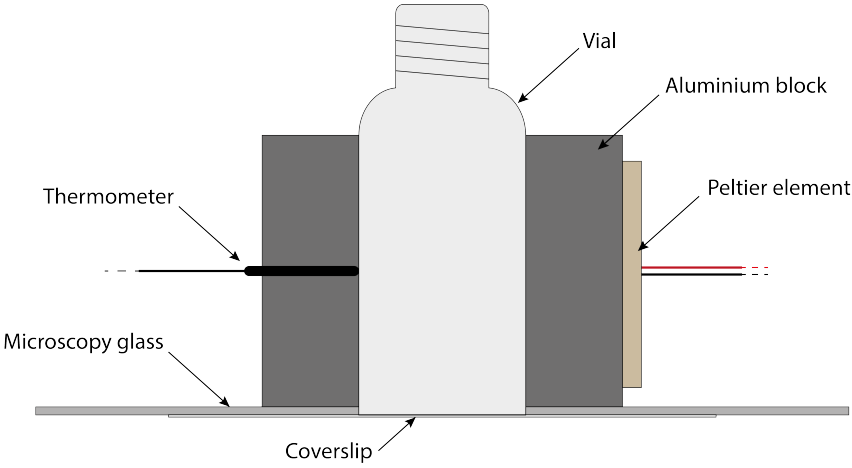

Fig. 3.3: Schematic representation of the sample cell used for microscopy experiments.

density than water, so they sink to the bottom of the vial, resulting in effective two-dimensional motion.

The exposure time and LED strength were adjusted for optimal contrast between particles and background. Typically, the exposure time was set to 33.3 ms to obtain a frame rate of exactly 30 fps, with the LED strength set to 10 %. For the video recording, the 'Fast TimeLapse' function of NIS Elements was used, the output video was in *.nd2* format. Prior to use for particle tracking, the file was converted to an 8-bit TIFF stack. The software ImageJ was used for this, using the function 'Process > Batch > Convert...'.

3.5.3 Particle tracking

The obtained TIFF stack was loaded into MATLAB, and a custom code by Blair and Dufresne determined the particle positions in each frame and linked them together to form individual trajectories. The tracking code is shown in Appendix C. This code outputs a text file for each video with particle X-position, Y-position, particle number and frame number. This output file is used for further analysis.

The parameters used in the trackingcode (for our particles at 60x

magnification, 30–60 fps) are as follows (see also Appendix C):

```
diameter=25;     % average diameter of a 'particle' (a.u.)
threshold=25;    % minimum brightness of a 'particle' (a.u.)
maxdisp=10;      % maximum step size (in pixels)
param.mem=3;     % how long particle can go missing (frames)
param.dim=2;     % dimensionality of data (2-dimensional)
param.good=50;   % how long track needs be to be accepted (frames)
```

The above parameters must be adjusted for different particle size, magnification or frame rate.

3.6 Analysis

For the most part, analysis was performed using the program MATLAB (version R2015a), which allows for the use of large data sets and image analysis.

3.6.1 Mean squared displacement

From the particle trajectories, the mean squared displacement is calculated by first calculating the squared displacement:

$$\mathrm{SD} = (x(t+\Delta t) - x(t))^2 + (y(t+\Delta t) - y(t))^2 \tag{3.1}$$

with x and y the x- and y-position, respectively, and Δt the time step.

First, we obtain all displacements at $\Delta t = 1$ (so from frame 1–2, 2–3, 3–4,...) and average. This is MSD(1). Then we do the same for $\Delta t = 2$ (1–3, 2–4, 3–5,...) and for $\Delta t = 3$ (1–4, 2–5, 3–6,...) and so on. The mean squared displacement is obtained for every Δt. Typically we average over 10–20 particles of the same experiment [17, 10].

One important implication to note is that at higher Δt, there are less data points (for example, if $t_{max} = 1000$, $\Delta t = 999$ will only give two points; $t = 1$ and $t = 2$). Therefore, the statistics become less and less reliable at higher Δt. For this reason, only time-steps up to $\Delta t = t_{max}/2$ are used for analysis, as the optimum between number of data points and reliability of the data points. Typically, the first 200 frames of the MSD from a track of at least 600 frames are used for data fitting. The MATLAB code is shown in Appendix D.

3.6.2 Velocity autocorrelation

The velocity autocorrelation is calculated from the particle trajectories. From a trajectory, the instantaneous velocity is calculated for time t and for $t + \Delta t$. The autocorrelation θ between $v(t)$ and $v(t + \Delta t)$ is then calculated via:

$$\theta(t, \Delta t) = \frac{b + c - a}{2\sqrt{b \cdot c}} \tag{3.2}$$

with

$$a = (v_y(t + \Delta t) - v_y(t))^2 + (v_x(t + \Delta t) - v_x(t))^2$$
$$b = v^2(t)$$
$$c = v^2(t + \Delta t).$$

The obtained $\theta(t + \Delta t)$ are averaged over every starting time t to give $\phi(\Delta t)$ and the same is done for the next time-steps Δt up to $t_{max}/2$. Finally, the autocorrelation is typically averaged over 10–20 particles of the same experiment, as with the mean squared displacement. The MATLAB code is shown in Appendix E.

3.7 Rheometry

Rheometry was used to determine the viscosity of hydrogen peroxide/water mixtures at various temperatures. A Paar Physica MCR 300 modular compact rheometer was used with a CP50-1 cone-plate (50 mm diameter, 1° cone) and the software Rheoplus V3.40. The shear rate was measured on a log ramp from 1–300 s^{-1}, from which the viscosity was calculated by the software at the point where the shear rate was constant.

Concentrations of 0 %, 1 %, 2 %, 5 % and 10 % H_2O_2 were tested at temperatures 20 °C, 24 °C, 27 °C, 30 °C and 33 °C. For each measurement, a fresh sample was used, because H_2O_2 reacted with the steel of the rheometer plate, forming oxygen bubbles after a few minutes which affected the measurement. Replacing the water/H_2O_2 mixture for each measurement circumvented this problem.

4. RESULTS & DISCUSSION

4.1 Synthesis results

Silica-coated haematite superballs with a mean edge length of 983 nm and a polydispersity of 2.9 % were synthesised. The mean size and polydispersity of the synthesised particles were determined by transmission electron microscopy (TEM) imaging and subsequent size measurement with the software iTEM. The results are shown in Table 4.1. Representative TEM-images are shown for the particles HCII and Si@HCII in Figures 4.1 and 4.2. The shape factor m was determined by TEM measurement and contour fitting in MATLAB. While the polydispersity in size is small, the variation in shape is larger (roughly 25 %). This variation might lead to deviations in active motion later on.

The quality of the particle monolayer deposition was checked with scanning electron microscopy (SEM) or optical microscopy. The selection criteria were: a high particle packing density, most particles should lay flat on the glass surface and no multiple layers should be formed. After several attempts, suitable monolayers were formed, as can be seen in Figure 4.3. Generally, there were some dilute monolayer areas (a), some close-packed monolayer areas (b), and a few areas with double or triple layers of particles (c,d). For platinum coating, the depositions with mostly dilute or close-packed monolayer areas (checked with optical microscopy) were used.

To verify the presence of platinum on the superballs after sputter coat-

Tab. 4.1: Size statistics of synthesised particles.

Code	Mean edge length (nm)	Polydispersity (%)	m-value
HC2	862	3.1	-
Si@HC2	983	2.9	3.07 ± 0.8

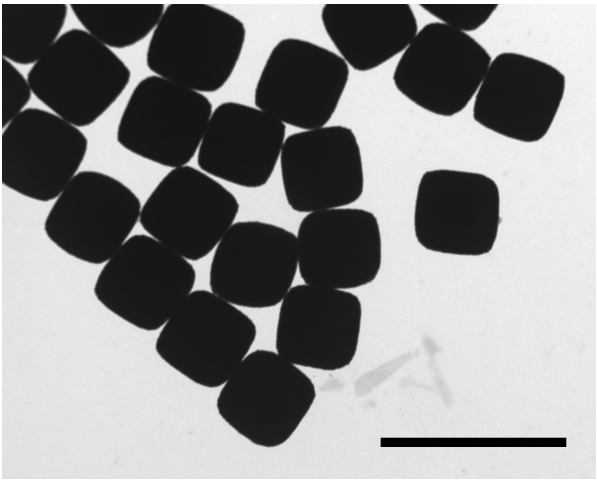

Fig. 4.1: Representative TEM image of HC2 haematite cubes. Scale bar is 2 µm. Particle edge length = 862 nm.

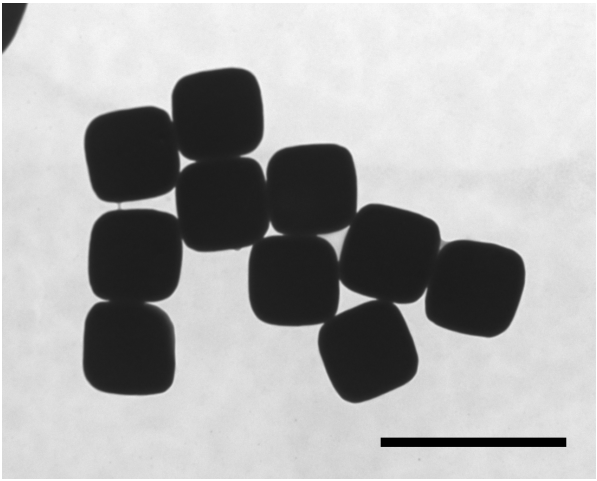

Fig. 4.2: Representative TEM image of Si@HC2 silica-coated haematite cubes. Scale bar is 2 µm. Particle edge length = 983 nm, $m = 3.07$. The silica layer is 50 nm thick. The silica layer is only visible with TEM if the layer is very thick.

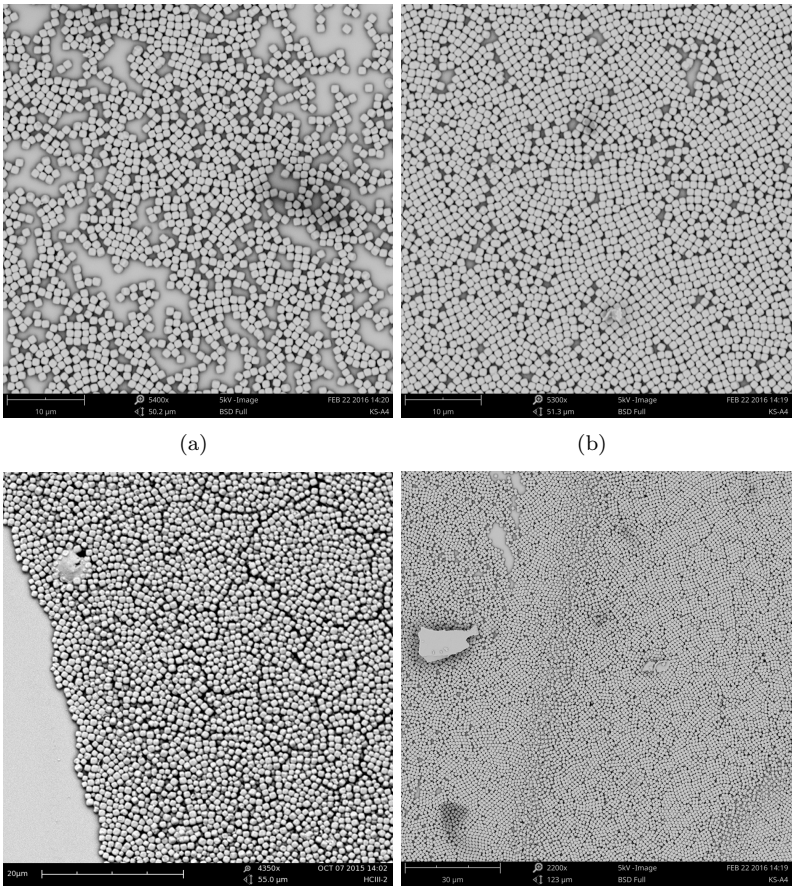

(a) (b)

(c) (d)

Fig. 4.3: SEM-images of a typical monolayer deposition result of silica-haematite superballs (Si@HC2) on a glass substrate. It shows (a) a dilute single layer, (b) a densely packed monolayer , (c) a multilayer structure and (d) a transition area from a single to a double layer.

ing, energy-dispersive X-ray spectroscopy (EDX) was performed on a sample. The resulting spectrum is shown in Figure 4.4. The Pt-peaks in the spectrum confirm the presence of platinum on the particles.

4.2 Swimming particles

The first experiments with Pt-coated silica particles consisted of adding a small aliquot of particle dispersion to water and observing their Brownian motion. Then, hydrogen peroxide (20%) was added to the dispersion, and the sample was briefly stirred. An increase in motion was expected, but all particles were immediately attached to the bottom of the glass. The sticking of particles to the glass was only briefly prevented by sonicating the mixture of particles with H_2O_2 and water prior to experiments. The pH of the H_2O_2/water mixture was tested to be 5, so it was concluded that the acidity of the solution caused the silica particles to lose stability.

Therefore, an amount of tetramethylammonium hydroxide (TMAH) was added as a base in order to set the pH to 8, the pH where silica is most stable [38]. At lower pH, silica becomes less negatively charged, so the repulsion between particles and glass and between each other becomes weaker. At pH higher than 8, there is an increasing chance of covalent bonding between the silica shell and the glass [38, 39].

Finally, the first active motion was observed for Pt-particles in 5% H_2O_2, showing clearly enhanced Brownian motion and short-term ballistic motion for most particles.

The experiment with Pt-coated particles in 5% H_2O_2 was initially performed for both silica-haematite particles and hollow silica particles. One advantage of using the hollow silica superballs instead of the silica-haematite particles was that the platinum side is distinguishable from the rest of the particle. This could help in determining whether or not a particle is coated with platinum, particularly useful if a particle is not moving. However, since particles are not active without platinum, we can safely assume there is platinum present if active motion is observed, so using hollow particles is not necessary.

The microscopy contrast for hollow particles proved insufficient to perform particle tracking. The difference in contrast can be seen in Figure 4.5; while the hollow particles with platinum appear to be quite visible to the eye, the contrast of these particles was too low for the tracking software. Hence, all further experiments were performed with only the silica-haematite particles.

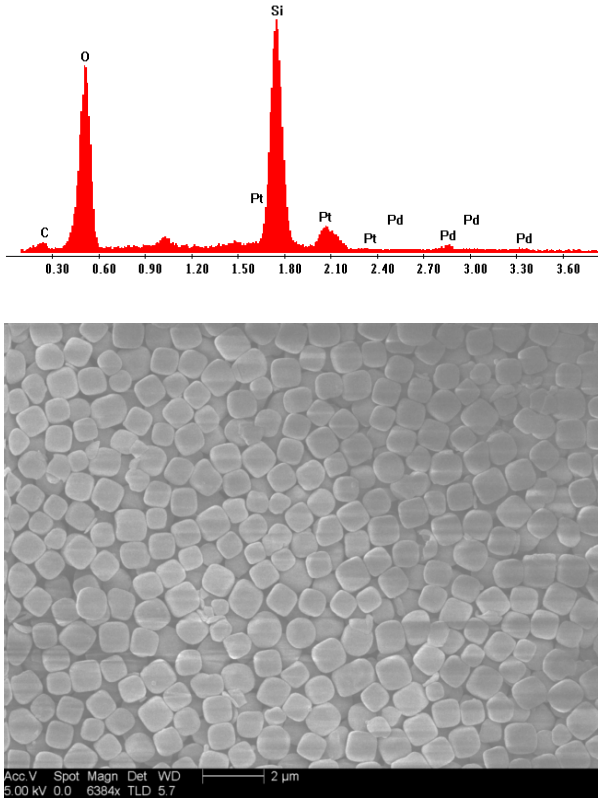

Fig. 4.4: Top: EDX spectrum of silica-coated haematite cubes coated with platinum. On the x-axis is the X-ray energy in keV, the y-axis is the number of counts in arbitrary units. Bottom: the corresponding SEM image.

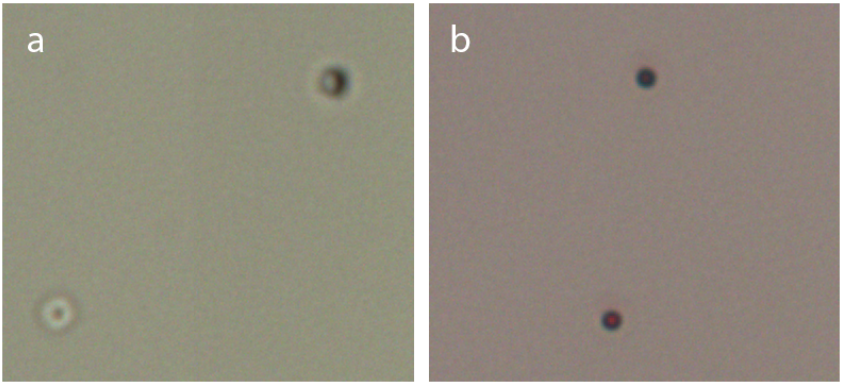

Fig. 4.5: (a) Hollow silica particles, one coated with platinum (top right), the other without platinum. (b) Silica-haematite particles, the platinum layer is not distinguishable.

4.3 Particle tracking

The optimal microscope magnification for particle tracking was determined by recording a few test videos and subsequently running the tracking code. A higher magnification yielded generally a clearer view of the individual particles, but the particles would swim out of view in just a few seconds, especially in higher H_2O_2 concentrations and at elevated temperatures. In addition, the particles moved in and out of focus more quickly on higher magnifications, causing the particles to 'disappear' every so often, causing the particle trajectories to be too short for analysis. At 40x or lower, the accuracy of the particle positions determined by the tracking code is too low. After several test experiments, it was concluded that using 60x magnification was the optimal trade-off between resolution and having the particles in the field of view long enough.

Typical particle trajectories at various H_2O_2 concentrations are shown in Figure 4.6. The parameters in the tracking code that proved optimal for particle tracking are listed in Section 3.5.3.

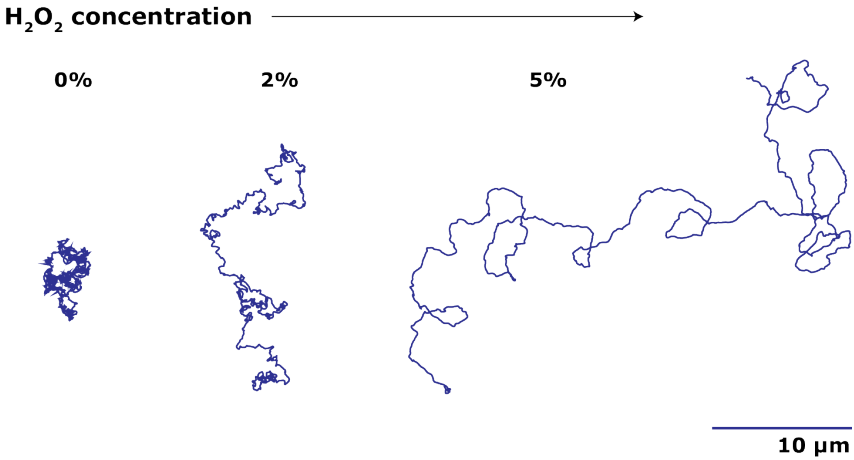

Fig. 4.6: Typical particle trajectories of Pt-coated superballs in different H_2O_2 concentrations in water at 24 °C. Increasing the H_2O_2 concentration increases active motion, causing the particle to cover more area in the same amount of time.

4.4 Diffusion coefficient

The Brownian diffusion coefficient of the non-active particles (Pt-particles in water, or non-Pt-particles in H_2O_2) was determined by taking the slope of their mean squared displacement versus time. The diffusion coefficient is then calculated as

$$D_0 = \frac{\langle R^2 \rangle}{4t}.$$

The results for various temperatures are shown in Table 4.2.

There is some variation between experiments at a certain temperature; for example at 25 °C, D_0 is calculated as $0.281\,\mu m^2\,s^{-1}$ for DvE_07-2 and $0.217\,\mu m^2\,s^{-1}$ for DvE_07-3. The cause of this variation may be due to for example small fluctuations in temperature.

Temperature control was used for all above-mentioned experiments, but for the experiments before September (DvE_09) the fluctuation was large, up to 1.0 °C. Only for the later experiments ('DvE_09-1' and on) the set-up was improved to obtain a temperature fluctuation of just 0.1 °C. These later experiments also yielded reproducible results, whereas the earlier experiments yielded varying results. Therefore, the values determined

Tab. 4.2: Diffusion coefficient determined by linear fitting of the mean squared displacement. Experiment codes correspond to different sets of experiments at different temperatures.

Experiment	T (°C)	D_0 ($\mu m^2\,s^{-1}$)
DvE_07-2	25 ± 1.0	0.281
DvE_07-3	25 ± 1.0	0.217
DvE_07-4	28 ± 1.0	0.253
DvE_08-1	24 ± 1.0	0.247
DvE_08-2	30 ± 1.0	0.336
DvE_09-1.1	24 ± 0.1	0.217
DvE_09-1.2	27 ± 0.1	0.287
DvE_09-1.3	30 ± 0.1	0.303
DvE_09-1.4	33 ± 0.1	0.352

from experiment DvE_09-1 onwards are considered the most trustworthy.

Small variations in particle size or shape can also play a large role in the variation in diffusion coefficient, since for the analysis only about 10–20 particles are taken into account. One or two particles that are larger or smaller than average can tip the value for diffusion significantly either way. The resolution of optical microscopy is not sufficient to determine the size of each particle, otherwise we could try to compensate for the size in de diffusion coefficient.

4.5 Effective diffusion

The effective diffusion coefficient is calculated in the same way as the Brownian diffusion coefficient, by taking the slope of the mean squared displacement versus time. For active particles, only the long-time MSD is taken into account, at $t \gg \tau$, assuming the particles move (enhanced) diffusively at long time scale. In practice, linear fitting was performed on the time interval $t = 4$–6 seconds, using the assumption that $\tau < 4\,s$. This interval is chosen because the MSD was generally linear in that range. At higher Δt the MSD tends to become less stable, as can be seen in Figure 4.7. D_{eff} is then calulated with:

$$D_{\text{eff}} = \frac{\langle R^2 \rangle}{4t}.$$

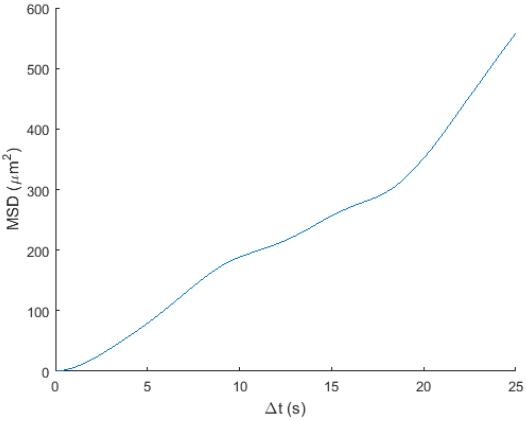

Fig. 4.7: Typical MSD of a single active particle, showing the increased instability at higher Δt, because there is less data per point. At $t < 6\,\mathrm{s}$ and $t > 4\,\mathrm{s}$, the MSD is generally linear.

The results are shown in Figure 4.8.

It is clear that the effective diffusion increases with both fuel concentration and with temperature. A higher fuel concentration corresponds with higher propulsion force, since more H_2O_2 is being decomposed at the platinum surface, causing the local concentration gradient to become stronger. An increase in temperature also enhances the effective diffusion, because the viscosity of the fluid decreases (see Section 4.8) and the H_2O_2 decomposition reaction rate increases [40].

One interesting point to note is that D_{eff} at 24 °C is higher for 1 % H_2O_2 than for 2 % H_2O_2. This is most probably an error in the experiment, since for the 1 % experiment the sample was heated to 30 °C before cooling down to 24 °C. The sample might not have been cooled thoroughly before the experiment, leading to increased diffusion.

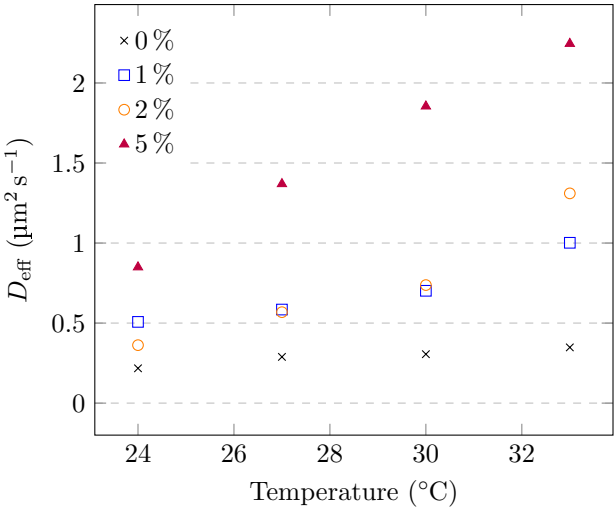

Fig. 4.8: Effective diffusion coefficient of active particles at various H_2O_2 concentrations versus temperature, determined by fitting equation 2.9 to Δt = 4–6 s of the MSD. D_{eff} increases with both temperature and H_2O_2 concentration.

4.6 Swimming velocity

This section will treat the velocity of the active particles as function of temperature and fuel concentration. The velocity is calculated in three ways: by taking the mean displacement between each frame, by fitting the start of the MSD with equation 2.8, and by fitting equation 2.7 to the entire MSD curve.

4.6.1 Mean displacement

First, the instantaneous velocity is calculated by taking the mean absolute displacement of a particle between each frame. The swimming velocity, *i.e.* the active part of the velocity, is then determined by subtracting the velocity of Brownian particles at the same temperature. The effect of the different viscosity of H_2O_2 compared to water is neglected, because the change in viscosity is found to be minimal (see section 4.8).

To illustrate: a particle in water has a mean velocity of $6.31\,\mu m\,s^{-1}$ at 24 °C. An active particle (in 2 % H_2O_2) has a mean velocity of $7.71\,\mu m\,s^{-1}$ at 24 °C, so the swimming velocity at 2 % H_2O_2 is $1.4\,\mu m\,s^{-1}$. The results are shown in Figure 4.9.

This method is suspected to be the least reliable of the three. This is inherent to its nature; particle tracking gives the position of the particles only up to a certain resolution (about 0.11 µm/px, the resolution of the microscope) and the displacement between two frames is typically in the range of 1–10 pixels. To calculate the mean velocity, this value is then multiplied by the frame rate, further increasing its error. For example, a mean displacement of 1 pixel per frame yields a mean velocity of $3.3\,\mu m\,s^{-1}$ at 30 fps. Therefore, the value $v = 1.4\,\mu m\,s^{-1}$ for 2 % at 24 °C is probably unreliable, since it goes beyond the resolution of the microscope.

Even so, upon adding H_2O_2, the mean velocity appears to increase. However, upon going from 2 % to 5 %, the velocity seems to decrease at higher temperatures, which is unlike what can be observed visually.

It is concluded that using the mean frame-to-frame displacement is an unfit method for determining the swimming velocity.

4.6.2 Quadratic fit

The swimming velocity can also be calculated by fitting the first 25 frames of the mean squared displacement to equation 2.8. Figure 4.10 shows a

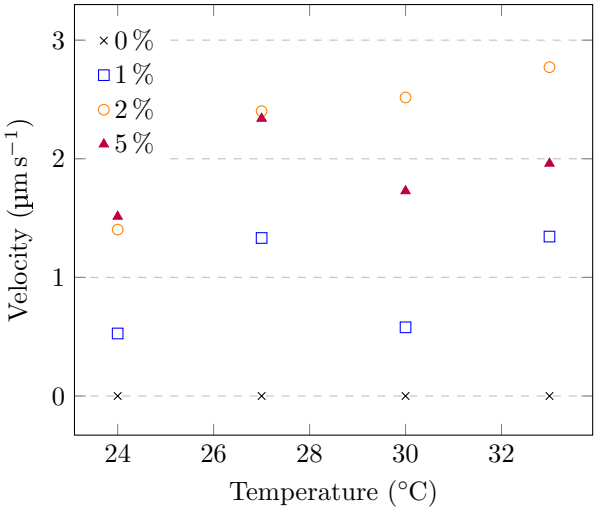

Fig. 4.9: Particle mean velocity at various H_2O_2 concentrations versus temperature, determined by taking the mean absolute displacement between each frame, minus the velocity in 0 % H_2O_2.

quadratic fit to an artificial data set, for illustrative purposes.

Figure 4.11 shows the swimming velocity versus temperature of active particles at various fuel concentrations. Since the short-time MSD can be fitted with a quadratic function, this confirms that the particles indeed show ballistic motion at short time scale, and not just enhanced diffusive motion. The same trend is seen for the velocity as for the effective diffusion, with the velocity increasing with fuel concentration and temperature, as expected.

As discussed before in section 2.2.4, Figure 2.3, platinum Janus spheres also showed this relation of velocity increasing with H_2O_2 concentration. In this respect, our self-propelling superballs behave similarly to spherical active particles.

The quadratic fit method, in contrast to the mean displacement method, gives plausible and reproducible results. Therefore, this method is considered to be a valid method for determining swimming velocity of active particles. This method will also be used later to determine the persistence time.

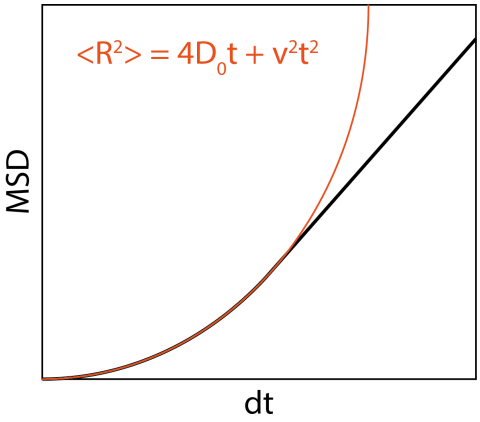

Fig. 4.10: Illustration of fitting equation 2.8 to the mean squared displacement. Orange line is the fit, black line is the 'data'.

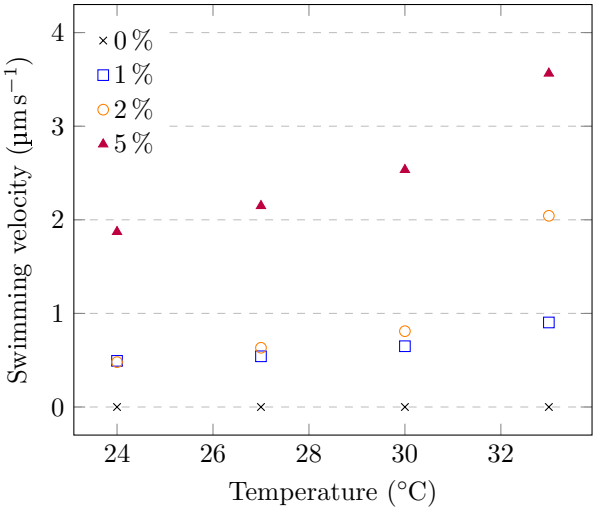

Fig. 4.11: Particle mean velocity at various H_2O_2 concentrations versus temperature, determined by fitting the first 25 frames of the MSD to equation 2.8.

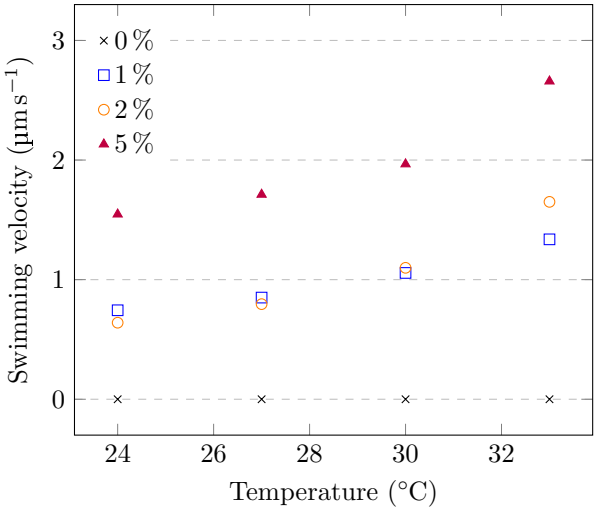

Fig. 4.12: Average swimming velocity at various H_2O_2 concentrations versus temperature, determined by fitting equation 2.7 to the measured MSD.

4.6.3 Full-range fit

The swimming velocity can also be determined by fitting the full range mean squared displacement with equation 2.7, listed here again for convenience:

$$\langle \mathbf{r}^2 \rangle = 4 \left(D_0 + \frac{1}{4} v^2 \tau \right) t + v^2 \tau \left[e^{-\frac{2t}{\tau}} - 1 \right]$$

D_0 is kept constant during fitting, using the value from linear fitting of the 0 % H_2O_2 data, i.e. the data from 'DvE_09-1' in Table 4.2. v and τ are the fit parameters.

The resulting swimming velocity versus T is shown in Figure 4.12. The general trend appears to be the same for both methods (the swimming velocity increases with fuel concentration and temperature), but the details are different. For example, a particle in 5 % H_2O_2 at 33 °C has a velocity of about 2.7 µm s^{-1}, whereas using the quadratic fit method this same particle's velocity was determined at 3.8 µm s^{-1}. Moreover, the specific values for the velocity at all data points are different between the two methods, while the positive trend is visible in both.

Both the quadratic fit and the full-range fit methods yield plausible results for the swimming velocity, in the order of a few micrometers per second. The latter has the advantage of fitting the entire range of the MSD, thus it more closely represents the actual data. However, the full-range fit also involves one extra fit parameter, decreasing the reliability of the value for v and τ. One way to circumvent the problem of an extra fit parameter, is to choose a constant value for the persistence time τ. This way, the only fit parameter is the velocity v. However, determining the value for τ already proves a challenge in itself.

4.7 Persistence time

The swimming velocity of active superballs showed a relation similar to that of spherical active particles [10, 17]. Now, we will cover the persistence time in a similar fashion to Section 4.6. It is calculated in three ways: from the velocity autocorrelation function (VAF); from fitting equation 2.8 to the short-time MSD and locating the point where the fit differs from the actual data; and by fitting equation 2.7 to the entire MSD.

4.7.1 Velocity autocorrelation function

The velocity autocorrelation function C_v is estimated as an exponential decay [41]: $C_\mathrm{v} \approx \mathrm{e}^{-t/\tau}$. Fitting the measured autocorrelation to this equation gives a value for the persistence length τ. However, the autocorrelation function in MATLAB did not work; it found no autocorrelation for any of the swimming particles. Several variants of the function were tried as well, to no avail. The obtained results for random and persistent particles were exactly the same. Therefore, the persistence time could not be determined by fitting the C_v.

4.7.2 Quadratic fit

The persistence time is determined here by taking the velocity as in Section 4.6.3, and finding the point where the quadratic fit differs from the actual data. This point in time is the typical time-step where particles move from ballistic motion to enhanced diffusive motion; the persistence length.

For the threshold for the difference between fit and data we chose e^{-1} as a set value. The exact value of this threshold does not significantly influence the obtained persistence time; a threshold of 0.2 or 2.0 yields generally the same result. The persistence time τ is determined as the point in time where:

$$(4D_0\Delta t + v^2\Delta t^2) - \left\langle R^2 \right\rangle \geq \mathrm{e}^{-1}$$

as illustrated in Figure 4.13. The results are shown in Figure 4.14.

The persistence time appears to decrease with temperature. In the case that persistence time is related to rotational diffusion of the particle, this makes sense, because the rotation time τ_R also decreases with temperature (see equation 2.4). Increasing the concentration of H_2O_2 seems

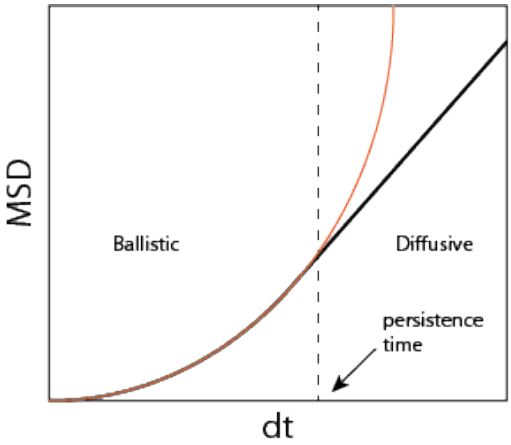

Fig. 4.13: Illustration showing the mean squared displacement going from ballistic (MSD $\sim t^2$) to diffusive (MSD $\sim t$). The point at which the fit and the data diverge is defined as the persistence length. (Image for illustrative purposes only, hence no units are shown).

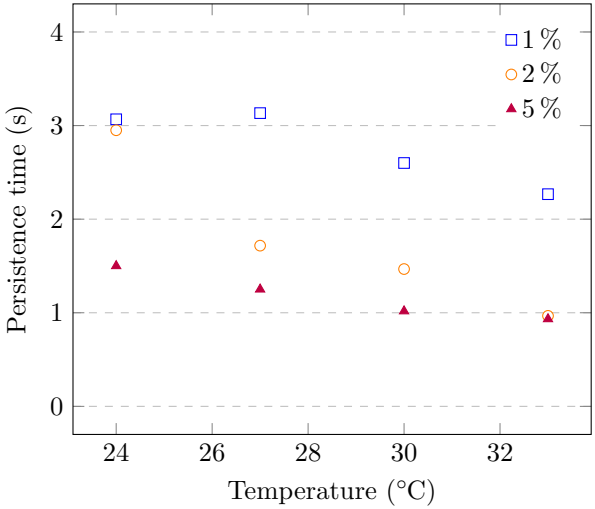

Fig. 4.14: Average persistence time at various H_2O_2 concentrations versus temperature, determined as the point where the fit of equation 2.8 differs more than e^{-1} from the measured MSD.

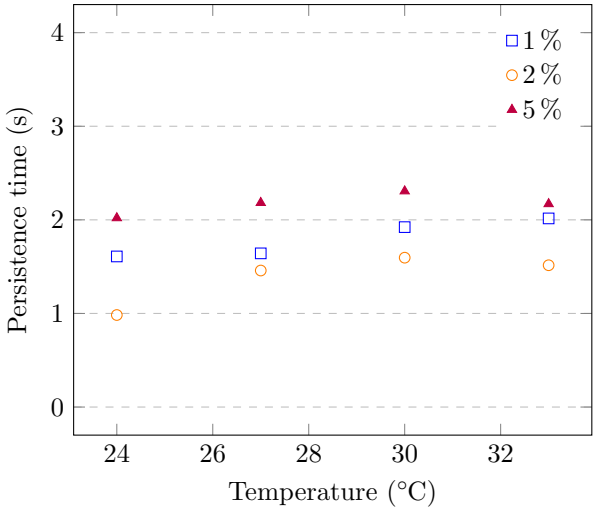

Fig. 4.15: Average persistence time at various H_2O_2 concentrations versus temperature, determined by fitting equation 2.7 to the measured MSD.

to decrease τ as well, which is less intuitive. An explanation for this decrease could be that the viscosity of the medium decreases with H_2O_2 concentration, which would lead to a shorter rotation time τ_R. However, as will be shown in section 4.8, viscosity *increases* with H_2O_2 concentration, and only slightly. The effect of viscosity is not sufficient to influence the rotation time (and thus, the persistence time) significantly.

It was shown in the previous section that swimming velocity increases with H_2O_2 concentration. Therefore, it must be concluded that the shorter persistence time is caused by the increased swimming velocity.

4.7.3 Full-range fit

The persistence time can also be determined by fitting the mean squared displacement with equation 2.7. As explained in section 4.6.3, the velocity will be kept constant for the fit (for a set temperature and H_2O_2 concentration), at the value obtained from the quadratic fit. The resulting persistence time versus temperature is shown in Figure 4.15.

The persistence time appears to be shorter for 2 % H_2O_2 than for 1 %, but again longer for 5 %, unlike what was seen in Figure 4.14. There

does not appear to be a trend in persistence time with either temperature or H_2O_2 concentration. If anything, the persistence time appears to increase slightly with temperature, while the rotational diffusion time should decrease at higher temperatures.

4.7.4 Discussion

The quadratic fit method yielded a negative relation between persistence time and temperature, as is expected, but the full-range fit method did not yield such a relation. Based solely on this, the quadratic fit gives a more plausible result. However, if the persistence time obtained with the quadratic fit is indeed accurate, this would mean that τ would decrease in higher H_2O_2 concentrations. Since the effect of viscosity is negligible (see section 4.8), the only factor is the swimming velocity. This would mean that the rotation time of the active particles is dependent on the swimming velocity, and not only on rotational diffusion. To the best of our knowledge, this relation is not seen for spherical active particles and could indicate an interesting property of self-propelling superballs.

However, we cannot say for sure which of the two methods is more accurate for determining τ. If we could use the velocity autocorrelation (section 4.7.1) and compare the obtained values with the two methods, we might be able to verify or falsify one of the methods. Then, the persistence time of superballs of different shape factors could be investigated. If the effect of swimming velocity on persistence time is more pronounced for more cube-like particles, that would also verify the observation. A theoretical description of the rotation of superball-shaped particles moving at different velocities would be interesting as well, to compare with the measured data.

4.8 Viscosity of hydrogen peroxide solutions

The viscosity of various concentrations of hydrogen peroxide solutions in water is determined with rheology. The results are shown in Figure 4.16. These values are used to calculate the theoretical value of the particles' rotational and translational diffusion coefficients.

It can be seen that for 1 % and 2 % H_2O_2, the viscosity is indistinguishable from that of pure water. For 5 % and 10 %, however, the viscosity goes slightly up, with the effect becoming even more pronounced at higher temperatures.

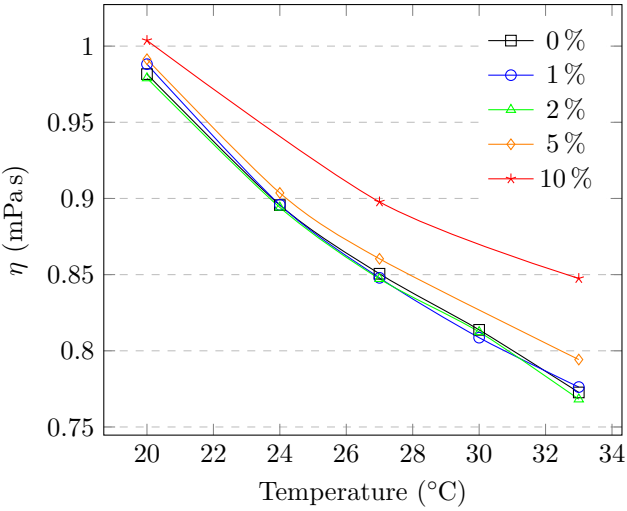

Fig. 4.16: Viscosity of various concentrations hydrogen peroxide solutions in water versus temperature, measured via rheology.

For spherical particles with $R = 1\,\mu m$, it is possible to calculate the theoretical values of the translational diffusion coefficient (D_0) and the rotational diffusion time ($\tau_R = D_R^{-1}$) at each temperature and H_2O_2 concentration by using the measured values for viscosity in Equations 2.3 and 2.4, respectively. As discussed before, in section 2.2.3, the difference in diffusion coefficient between spheres and superballs is not significant. Therefore, the calculated diffusion coefficients for spheres are a expected to be a good approximation for those of superballs. The results are shown in Figure 4.17 for concentrations up to 5 % H_2O_2, as that was the highest concentration used in the self-propulsion experiments.

For 0 %, 1 % and 2 % H_2O_2, there is no significant difference in the diffusion coefficient or in the rotation time. Particles in 5 % H_2O_2 diffuse slightly slower, because the viscosity is slightly higher. This result confirms that the effect of H_2O_2 concentration on viscosity can be neglected in the self-propulsion experiments.

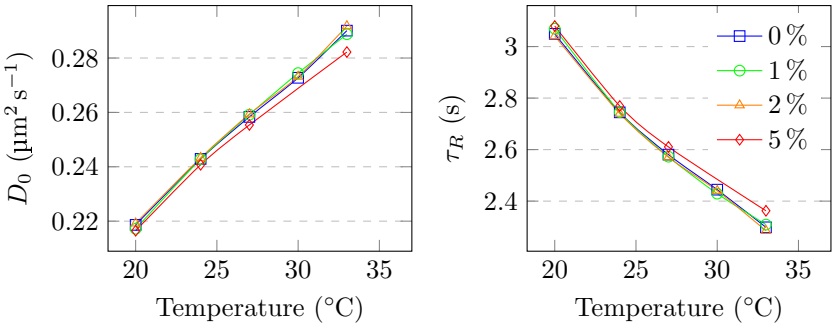

(a) (b)

Fig. 4.17: (a) Brownian diffusion coefficient D_0 and (b) rotational relaxation time τ_R of spherical particles of radius 1 µm in various concentrations H_2O_2 in water at different temperatures, calculated using equation 2.3 and 2.4 with experimentally determined values for the viscosity of the water/H_2O_2 mixture.

5. CONCLUSION

In this thesis, the first steps are taken towards characterising the effect of particle cubicity on its active motion.

Superball-shaped colloids, consisting of a haematite core with a silica shell were successfully synthesised. The synthesised particles had an edge length of 980 nm with a size polydispersity of 3 % and a shape factor $m = 3$. A monolayer of these particles was deposited and subsequently coated with platinum. After dispersing the Pt-coated particles in hydrogen peroxide solutions, the particles showed self-propelling motion.

We showed that at short times, the self-propelling particles moved ballistically, going to diffusively at longer time scales with a higher effective diffusion coefficient. Furthermore, it was shown that the effective diffusion and the swimming velocity increase with H_2O_2 concentration and temperature, similar to spherical active particles.

Two methods were proposed to determine the persistence time. A quadratic fit resulted in a decreasing persistence time with temperature and H_2O_2 concentration, while the full-range fit yielded no clear relation. If there is indeed a relation between swimming velocity and the persistence time, as implied by the quadratic fit method, this would indicate an interesting property unique to active superball colloids. However, as there is no way of determining which of the two methods is more trustworthy, no quantitative conclusions can be drawn yet about the persistence time and how it is affected by temperature, swimming velocity or cubicity. A more reliable method needs to be developed for accurately quantifying the persistence time.

6. OUTLOOK

Research on self-propelling superballs is far from complete, there is still very much that can be done. Some suggestions for further research, in no particular order:

- A more robust system could be developed for measuring active motion, for example using microfluidics [42]. It is possible to create a continuous inflow of hydrogen peroxide, so that the fuel concentration is constant over time.
- Microfluidics could also be used to gradually increase the fuel concentration during an experiment, which could be used to map the swimming behaviour as function of fuel concentration in more detail.
- A more reliable/precise method for platinum-coating might be useful, for example E-beam physical vapor deposition.
- The thickness of the platinum layer could be varied to study how it affects active motion.
- Various particle sizes could be investigated to see how size affects active motion.
- Instead of platinum, the enzyme catalase could be used to decompose H_2O_2, since catalase is known to decompose hydrogen peroxide much faster than platinum [43, 44]. In this way, self-propulsion might be achieved at much lower fuel concentrations, further increasing the applicability of this system.
- The propulsion force of an individual particle can be measured using optical tweezers, as in ref [44]. This way, the propulsion force can be measured independently as a function of H_2O_2 concentration and temperature.

- The self-assembly of active superballs is a very interesting research direction.
- The rotational diffusion of the superballs can be measured (for instance with FRAP-DLS) for comparison with the obtained persistence time.
- The three-dimensional motion could be studied, for instance using a fluorescent dye with confocal microscopy. The particles are quite dense compared to water, so keeping them dispersed might be a problem. Perhaps this can be compensated (partly) by using a different solvent with a higher density.
- Magnetic fields could be used to 'steer' the swimming particles through a solution. For example, a micron-sized labyrinth could be created via soft lithography, through which the particle has to manoeuvre.
- Magnetic fields could also form linear chains of magnetic colloids, with an active cap at one end. This forms so-called 'colloidal trains', which might be used to model the swimming motion of flagellates.

7. ACKNOWLEDGEMENTS

I would like to take this opportunity to thank some people who helped me create this thesis. First of all, I would like to thank Samia for daily supervision and teaching me how to be a researcher. Second, I'd like to thank Andrei, for being my second supervisor, and for always being enthusiastic about my research and having nice discussions and candies. Third, Albert Phillipse, for being my third supervisor.

Thank you to: everyone in the Crystal (Candy) Club; Chris Evers for all the help with optical microscopy; Pepijn, I couldn't have tracked the particles without your help; Chris Scheijdenberg for always helping me with the sputter coater and the SEM; Bonnie for investing a lot of time in developing the heating set-up; Dominique for the help with rheology and for agreeing to be my examiner for the internship; Fuqiang and Kanvaly for supervision when Samia was away.

Then I would like to thank my fellow master students and the rest of the FCC group for being very nice and for all the cookies and cakes! Mam, pap, Sander, dankjewel voor jullie steun :)

Finally, Anne, thank you for your limitless love and support ♡.

BIBLIOGRAPHY

[1] S. J. Ebbens, "Active colloids : Progress and challenges towards realising autonomous applications," *Current Opinion in Colloid & Interface Science*, vol. 21, p. 14, 2016.

[2] E. M. Purcell, "Life at low Reynolds number," *American Journal of Physics*, vol. 45, p. 3, 1977.

[3] E. Lushi, H. Wioland, and R. E. Goldstein, "Fluid flows created by swimming bacteria drive self-organization in confined suspensions.," *Proceedings of the National Academy of Sciences of the United States of America*, vol. 111, no. 27, p. 9733, 2014.

[4] I. H. Riedel, K. Kruse, and J. Howard, "A Self-Organized Vortex Array of Hydrodynamically Entrained Sperm Cells," *Science*, vol. 309, no. 8, p. 300, 2005.

[5] G. M. Viswanathan, "Lévy flight search patterns of wandering albatrosses," *Letters to Nature*, vol. 381, p. 413, 1996.

[6] G. M. Viswanathan, "Fish in Lévy-flight foraging Expanding islands of speciation," *Nature*, vol. 465, p. 1018, 2010.

[7] D. Brockmann, L. Hufnagel, and T. Geisel, "The scaling laws of human travel," *Nature Letters*, vol. 439, no. January, p. 4, 2006.

[8] L. Baraban, D. Makarov, R. Streubel, I. Mönch, D. Grimm, S. Sanchez, and O. G. Schmidt, "Catalytic Janus motors on microfluidic chip: Deterministic motion for targeted cargo delivery," *ACS Nano*, vol. 6, p. 3383, apr 2012.

[9] J. R. Baylis, J. H. Yeon, M. H. Thomson, A. Kazerooni, X. Wang, A. E. S. John, E. B. Lim, D. Chien, A. Lee, J. Q. Zhang, J. M. Piret,

L. S. Machan, T. F. Burke, N. J. White, and C. J. Kastrup, "Self-propelled particles that transport cargo through flowing blood and halt hemorrhage," *Science Advances*, vol. 1, no. 9, p. 1, 2015.

[10] H. Ke, S. Ye, R. L. Carroll, and K. Showalter, "Motion analysis of self-propelled Ptsilica particles in hydrogen peroxide solutions," *Journal of Physical Chemistry*, vol. 114, p. 5462, 2010.

[11] A. T. Brown and W. C. K. Poon, "Ionic effects in self-propelled Pt-coated Janus swimmers," *arXiv*, 2013.

[12] W. Wang, W. Duan, S. Ahmed, T. E. Mallouk, and A. Sen, "Small power: Autonomous nano- and micromotors propelled by self-generated gradients," *Nano Today*, vol. 8, no. 5, p. 531, 2013.

[13] L. Baraban, R. Streubel, D. Makarov, L. Han, D. Karnaushenko, O. G. Schmidt, and G. Cuniberti, "Fuel-free locomotion of janus motors: Magnetically induced thermophoresis," *ACS Nano*, vol. 7, p. 1360, feb 2013.

[14] R. Mhanna, F. Qiu, L. Zhang, Y. Ding, K. Sugihara, M. Zenobi-Wong, and B. J. Nelson, "Artificial bacterial flagella for remote-controlled targeted single-cell drug delivery," *Small*, vol. 10, no. 10, p. 1953, 2014.

[15] N. Koumakis, a. Lepore, C. Maggi, and R. Di Leonardo, "Targeted delivery of colloids by swimming bacteria.," *Nature communications*, vol. 4, p. 2588, 2013.

[16] J. Palacci, S. Sacanna, A. P. Steinberg, D. J. Pine, and P. M. Chaikin, "Living Crystals of Light-Activated Colloidal Surfers," *Science*, vol. 339, no. 6122, p. 936, 2013.

[17] J. R. Howse, R. a. L. Jones, A. J. Ryan, T. Gough, R. Vafabakhsh, and R. Golestanian, "Self-Motile Colloidal Particles: From Directed Propulsion to Random Walk," *Physical Review Letters*, vol. 99, no. 4, p. 8, 2007.

[18] K. Marx, *Self-propelled rod-like swimmers near surfaces*. PhD thesis, Universität zu Köln, 2011.

[19] S. Sanchez, L. Soler, and J. Katuri, "Chemically powered micro- and nanomotors," *Angewandte Chemie - International Edition*, vol. 54, no. 5, p. 1414, 2015.

[20] J. M. Meijer, D. V. Byelov, L. Rossi, A. Snigirev, I. Snigireva, A. P. Philipse, and A. V. Petukhov, "Self-assembly of colloidal hematite cubes: a microradian X-ray diffraction exploration of sedimentary crystals," *Soft Matter*, vol. 9, p. 10729, 2013.

[21] L. Rossi, *Colloidal superballs*. PhD thesis, Universiteit Utrecht, 2012.

[22] L. Rossi, V. Soni, D. J. Ashton, D. J. Pine, A. P. Philipse, and P. M. Chaikin, "Shape-sensitive crystallization in colloidal superball fluids," *PNAS*, 2015.

[23] T. Sugimoto, "Preparation of monodisperse peanut-type α-Fe_2O_3 particles from condensed ferric hydroxide gel," *Colloids and Surfaces A: Physicochemical and Engineering Aspects*, vol. 70, p. 167, 1993.

[24] C. Graf, D. L. J. Vossen, A. Imhof, and A. V. Blaaderen, "A General Method To Coat Colloidal Particles with Silica," *Langmuir*, vol. 19, no. 2, p. 6693, 2003.

[25] L. Rossi. Unpublished work, 2016.

[26] A. G. M. Brinkman, "Preparations and properties of colloidal cubes," tech. rep., Universiteit Utrecht, Utrecht, 2011.

[27] J. R. Royer, G. L. Burton, L. Blair, and S. D. Hudson, "Rheology and dynamics of colloidal superballs," *Soft Matter*, vol. 11, p. 5656, 2015.

[28] R. Tuinier. Private communication, 2016.

[29] K. Sekimoto, *Stochastic Energetics*. Springer-Verlag Berlin Heidelberg, 1 ed., 2010.

[30] B. V. Derjaguin, "Title unknown," *Kolloidnyi Zhurnal*, vol. 9, no. 5, p. 335, 1947.

[31] D. Velegol, A. Garg, R. Guha, A. Kar, and M. Kumar, "Origins of concentration gradients for diffusiophoresis," *Soft Matter*, vol. 12, p. 4686, 2016.

[32] D. Mac Innes, "The mechanism of the catalysis of the decomposition of hydrogen peroxide by colloidal platinum," *Journal of the American Chemical Society*, vol. 36, p. 878, 1914.

[33] A. T. Brown and W. C. K. Poon, "How platinum-coated Janus particles swim," *arXiv*, vol. 1, 2013.

[34] A. F. Ioffe, *Semiconductor Thermoelements and Thermoelectric Cooling*. Infosearch Limited, 1957.

[35] S. Castillo, *Cubic Colloids*. PhD thesis, Universiteit Utrecht, 2015.

[36] J. M. Meijer, *Colloidal Crystals of Spheres and Cubes in Real and Reciprocal Space*. PhD thesis, Universiteit Utrecht, 2015.

[37] F. Burmeister, W. Badowsky, T. Braun, S. Wieprich, J. Boneberg, and P. Leiderer, "Colloid monolayer lithography - A flexible approach for nanostructuring of surfaces," *Applied Surface Science*, no. 144-145, p. 461, 1999.

[38] R. Iler, *The Chemsitry of Silica*. New York, Chichester: John Wiley and Sons, 1979.

[39] R. Iler, *The Chemistry of Silica: Solubility, Polymerization, Colloid and Surface Properties and Biochemistry of Silica*. New York, Chichester: Wiley-Interscience, 1980.

[40] T. A. Vetter and D. P. Colombo, "Kinetics of Platinum-Catalyzed Decomposition of Hydrogen Peroxide," *Journal of Chemical Education*, vol. 80, no. 7, p. 788, 2003.

[41] K. J. Beers, *Numerical Methods for Chemical Engineering: Applications in MATLAB*. Cambridge University Press, 2007.

[42] J. Palacci, C. Cottin-Bizonne, C. Ybert, and L. Bocquet, "Sedimentation and Effective Temperature of Active Colloidal Suspensions," *Physical Review Letters*, vol. 105, 2010.

[43] P. T. Vasudevan and R. H. Weilandtt, "Studies on the morphology of immobilized catalase," *The Chemical Engineering Journal*, vol. 55, p. B41, 1994.

[44] X. Ma, A. Jannasch, U. R. Albrecht, K. Hahn, A. Miguel-López, E. Schäffer, and S. Sánchez, "Enzyme-Powered Hollow Mesoporous Janus Nanomotors," *Nano Letters*, vol. 15, no. 10, p. 7043, 2015.

APPENDIX

A. PRELIMINARY EXPERIMENTS DIFFERENT SHAPE FACTORS

A few preliminary experiments have been performed with three new particles with different m-value, to test the effect of cubicity. The following particles were used: silica spheres with $m = 2$ (935 nm), superballs with $m = 3.5$ (1033 nm) and superballs with $m = 3.8$ (1400 nm). Their self-propelling motion was studied at 27 °C in 5 % H_2O_2. This temperature and concentration was chosen because self-propulsion of our own particles was typically well pronounced at these values. The particles were coated with platinum in the same way as described previously. However, the sputter coated malfunctioned at this point (see Appendix B). Due to time constraints, the experiments could not be performed in time for this thesis.

For the platinum-coated silica spheres, the platinum half is clearly distinguishable from the non-coated half: the platinum side being black and the non-coated side being white. During microscopy experiments it was observed that for the most time, the particle appeared black, see Figure A.1. Since we use an inverted microscope, we see the bottom of the particle. This means that the platinum-coated side of the spheres was usually pointing downwards.

If that is indeed the case, it would explain why the particles do not show self-propelling behaviour, but instead appear to move Brownian. If the platinum side touches the glass at the bottom, there is much less area of platinum free to catalyse the decomposition of hydrogen peroxide. Moreover, the propulsion force generated in that case is pointed upward, and so does not contribute to the 2-dimensional motion of the particle. The propulsion force is probably not strong enough to actually propel the particle up from the glass, since the particles are too heavy.

To explain why the platinum side points downwards, we can estimate the mass of the platinum with respect to the total particle mass. If we take the diameter of the sphere as 935 nm, its volume is 4.28×10^{-13} cm^3. By

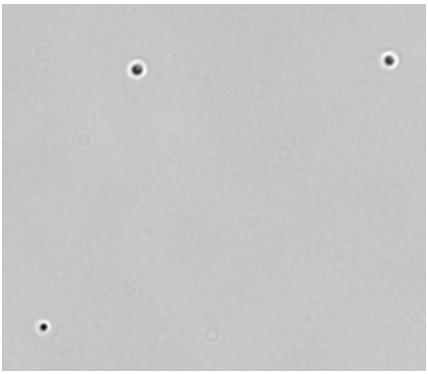

Fig. A.1: Three platinum-coated silica spheres in dispersion. The particles appear black, because the platinum-coated side is facing down, towards the camera.

multiplying this volume with the average density of Stöber silica (around $2\,\mathrm{g\,cm^{-3}}$) we get a mass per particle of roughly 1 pg (without platinum).

We can estimate the volume of platinum by taking the surface of half a sphere (since the particle is half-coated) and multiplying it by the thickness of the layer (5 nm). This yields a volume of $6.87 \times 10^{-15}\,\mathrm{cm^3}$, which, multiplied by the density of platinum ($21.45\,\mathrm{g\,cm^{-3}}$) yields a platinum mass of 0.147 pg. $0.147/(1 + 0.147) * 100\% = 12.8\%$, which means that just the thin platinum layer comprises 12.8% of the total mass of the particle.

For comparison, we can estimate the same for a silica-coated haematite cube (assuming a perfect cube for convenience). The total mass of a single cube without platinum is 4.55 pg. If only one face is coated with platinum (which is very plausible in reality at high enough m-value), the volume of platinum is $5.0 \times 10^{-15}\,\mathrm{cm^3}$, giving a mass of 0.107 pg. $0.107/(4.55 + 0.107) * 100\% = 2.3\%$, so only 2.3% of the total particle mass is platinum.

The relatively large mass of platinum on the silica spheres could explain why the platinum side generally drops downwards, while for the silica-haematite superballs it does not.

B. SPUTTER COATING

The sputter coater malfunctioned just as we started the previous preliminary experiments, it was unable to measure the thickness of the platinum. Therefore, for these experiments the platinum coating was unreliable. This had an effect on the self-propulsion of the particles; the swimming behaviour seen with our Pt-coated Si@HCII particles was not reproducible for these new particles. One batch of Pt-coated particles showed some propelled motion, but with very low velocity, other batches showed no propulsion at all.

Sputter coating is not quite ideal for synthesising reproducible self-propelling particles, as it seems to yield varying results with each coating procedure. This can be caused by the Pt-target degrading over multiple uses, causing irregularities in the coating, or by the inherent inaccuracy of the method. Sputter coating is usually used for preparation of samples for scanning electron microscopy (SEM), where a high quality platinum layer is not necessary.

For the purpose of following the motion of one batch of particles (so all particles have more or less the same amount of platinum), sputter coating is sufficient. However, to more quantitatively study the effect of shape factor on self-propulsion, we might need a more reliable method for platinum coating, for example electron beam physical vapor deposition (EBPVD).

C. TRACKINGCODE.M

This is the MATLAB code used for locating particle positions in every frame. It is a modified script, originally created by Daniel Blair and Eric Dufresne (website: http://site.physics.georgetown.edu/matlab/). Linking the positions to form a trajectory is done with the function 'track.m'. Track.m is not given in this thesis, as the code is too big to display on paper. Explanations for some steps are given in the comments in green, denoted by '%'.

```
a = [];
A=[];
pos=[];
radius=[];
% indicate name of tiffstack
fname = 'C:\Tiffstacks\stack 01.tif';
% indicate name under which to save output file
fsave = 'C:\Outputs\output 01.txt';

info = imfinfo(fname);
num_images = numel(info);
range = 1:num_images;

for k = range

    A = imread(fname, k);
    % set parameter for image analysis software here
    diameter=25;
    threshold=25;
    %set parameters for trackingsoftware here
    maxdisp=10; % maximum step size
    param.mem=3; % how long particle can go missing
    param.dim=2; % dimensionality of data
    param.good=50; % how long track needs be to be accepted
    param.quiet=0; % 0 = text, 1 = no text

    try
```

```
    ai=255-A;
    b=bpass(ai,1,diameter); % bandpass filter
    pk = pkfnd(b,threshold,diameter); % find peaks in intensity
    cnt = cntrd(b,pk,9);    % more accurate peak position (slow)
    cntl = length(cnt(:,1));
    radius=zeros(cntl,1)+5;
    cntpos = cnt(:,1:2);
    cntpos(:,3) = k;
    pos = [pos ; cntpos]; % write the particle positions

    catch
    disp('Error message: nothing above threshold.');
    disp('Script will continue anyway.');
    end

end

% link particle positions to form trajectory
tr=track(pos,maxdisp,param);

% saving the track to a .txt file
textfile=[tr];
fileID = fopen(fsave,'w');
fprintf(fileID , '%6.4f %6.4f %6.4f %6.4f \n' , textfile');
fclose(fileID);
```

D. MSD_CALC.M

This is the function used for calculating the mean squared displacement for each particle.

```
function [MSDtot] = msd_calc(input,fsave,pxsize)

%16-09-2015 Pepijn Moerman
%07-07-2016 Modified by Dennis van Eldik
%Aim: calculate the MSD of tracks
%input: text file containing: x ; y ; t ; particleID
%output: text file containing: lagtime ; MSD

Num=max(input(:,4));
MSDtot=[];
for i=1:Num
  count = find(input(:,4)==i);
  if ~isempty(count)
     a=input(count,1:3);
     tmax=length(a);
     MSD=[];
     STDEV=[];

     for t=1:tmax/2 % loop through time step dt
         SD=[];

         for q=1:tmax-1-t   % loop through t_0
             x1=a(q,1)*pxsize;  % MSD in micrometers
             y1=a(q,2)*pxsize;
             x2=a(q+t,1)*pxsize;
             y2=a(q+t,2)*pxsize;
             SD(q,1)=(x2-x1)^2+(y2-y1)^2; % squared displacement
         end

         MSD(t,1)=mean(SD); % mean squared displacement
         STDEV(t,1)=std(SD);
         MSD(t,2)=t;       % time step
         STDEV(t,2)=t;
```

```
    end

    l=length(MSD);
    p=length(MSDtot);
    MSDtot(p+1:p+l,1)=MSD(:,1);
    MSDtot(p+1:p+l,2)=STDEV(:,1);
    MSDtot(p+1:p+l,3)=i;
  end
end

% saving the MSD to a textfile, filename is given in 'fsave'
textfile=[MSDtot];
fileID = fopen(fsave,'w');
fprintf(fileID , '%6.4f %6.4f %6.4f\n' , textfile');
fclose(fileID);
```

E. VELOCITY_AUTOCORRELATION.M

```
function [phi] = phi_calc(input)
phi = [];
phi_low = [];
phi_high = [];
stdev = [];
particles = [];
time = [];

Alarge= input;
Alength=max(Alarge(:,4)); % number of trajectories in input

start=1;
stop=Alength;

for p=start:stop  % particle number
   count = find(Alarge(:,4)==p);
   A=Alarge(count,1:3); % take input for particle p
   l=length(A);
   stop2=l/2;
   % Test if this particle has a track
   if l>0
   % loop through time interval d
   for d=0:stop2  % d = 0 to half length trajectory
   theta=[];
      % loop through time i
      for i=1:l-2-(d+1) % due to how x and y are calculated
         x1= A(i,1);        % x-position at time i
         y1= A(i,2);        % y-position at time i
         x2 = A(i+1,1);     % x-position at time i+1
         y2 = A(i+1,2);     % y-position at time i+1
         x3 = A(i+d,1);     % x-position at time i+d
         y3 = A(i+d,2);     % y-position at time i+d
         x4 = A(i+d+1,1);   % x-position at time i+d+1
         y4 = A(i+d+1,2);   % y-position at time i+d+1
```

```
        xn1=x2-x1;          % instant x-velocity at time i
        yn1=y2-y1;          % instant y-velocity at time i
        xn2=x4-x3;          % instant x-velocity at time i+d
        yn2=y4-y3;          % instant y-velocity at time i+d

        % calculate difference in total v between time i and i+d
        a=(yn2-yn1)^2+(xn2-xn1)^2;

        b=xn1^2+yn1^2;      % total velocity at time i
        c=xn2^2+yn2^2;      % total velocity at time i+d

    % calculate the correlation between time i and i+d
        theta(i,1) = A(i,3);                    % frame number
        theta(i,2) = (b+c-a)/(2*sqrt(b*c));
     end
     if ~isempty(theta) % Only if theta is not empty
        phi((d+1),(p+1-start))=nanmean(theta(:,2));
        stdev((d+1),(p+1-start))=std(theta(:,2));
        phi_low(d+1,(p+1-start))=nanmean(theta(:,2))- ...
        std(theta(:,2));
        phi_high(d+1,(p+1-start))=nanmean(theta(:,2))+ ...
        std(theta(:,2));
     end
  end
  end

particles(p+1)= stop2;

end
```

F. LANGEVIN_FIT.M

This code fits the mean squared displacement with equation 2.7 to obtain values for v, l, τ and D_{eff}.

```
clear

fdir = 'F:\2016-09-13 results playfiles\july 4\exp 5\';
fps = 60;   % Frames per second
r_particle = 1.001E-6; % Particle RADIUS in m
tend = 200;
t = [1:1:tend]./fps;
setD0 = 0.252520431867606;
setD0std = 0;

Linearfit = 0;  % = 1 for non-active particles to get D_0

if Linearfit == 0
   ft = fittype( '4*(D_0 + (1/4)*l^2/tau)*t + l^2/tau* ...
   (exp(-2*t/tau)-1)','independent','t','dependent','y');
   lowerlimits = [setD0 0 0];
   upperlimits = [setD0 Inf Inf];
   startpoints = [setD0 1 1];
end

if Linearfit == 1
    ft = fittype( '4*D_0*t','independent','t','dependent','y');
    lowerlimits = [0];
    upperlimits = [Inf];
    startpoints = [0.3];
end

Rtot = [];
SDtot = [];
V_calc = [];
D_eff = [];

figure(3)
for particle = [1:400]
```

```
try

  fname = sprintf('%smsdparticle %i.txt',fdir,particle);
  R = textread(fname);
  R = R(1:end,:);
  r_length = length(R);

  if r_length >= tend
     SDtot = [SDtot R(1:1:tend,3)];
     Rtot = [Rtot R(1:1:tend,1)];
  end
  catch
     display(sprintf('Particle %i not found. Continuing...', ...
     particle));
  end
end

plot(t,mean(Rtot,2));
hold on
Weights = 1./mean(SDtot,2);
opts.Weigth = Weights;
[xData, yData] = prepareCurveData( t', mean(Rtot,2) );

if Linearfit == 0
   opts = fitoptions('Method','NonlinearLeastSquares', ...
   'Weight', Weights);
   opts.Display = 'Off';
   opts.Lower = lowerlimits;
   opts.Upper = upperlimits;
   opts.StartPoint = startpoints;
end

if Linearfit == 1
   opts = fitoptions( 'Method', 'NonlinearLeastSquares' );
   opts.Display = 'Off';
   opts.Lower = lowerlimits;
   opts.Upper = upperlimits;
   opts.StartPoint = startpoints;
end

[fitresult, gof,output] = fit( xData, yData, ft, opts );
MyCoeff = coeffvalues(fitresult);
CI = confint(fitresult,.60);
aD0 = MyCoeff(1);

if Linearfit == 1
    aD0std = CI(2,1)-aD0;
end
```

```
if Linearfit == 0
   al = MyCoeff(2);
   alstd = CI(2,2)-al;
   atau = MyCoeff(3);
   ataustd = CI(2,3)-atau;
   av = al/atau;
   avstd = av*(alstd/al + ataustd/atau);
   aDeff = aD0 + (1/4)*(al^2/atau);
   aDeffstd = setD0std + abs((1/4)*al*av*(alstd/al + avstd/av));
   % The desired coefficients will be given in a handy column:
   aaExcel = [aD0;setD0std;aDeff;aDeffstd;...
   al;alstd;atau;ataustd;av;avstd];
end

movegui([-25 -15]);
```